



Ministério da
**Ciência, Tecnologia
e Inovação**



sid.inpe.br/mtc-m21b/2014/01.23.11.02-TDI

EFFECT OF TRANSIENT GAS-PHASE ON FERROFLUID DROPLET VAPORIZATION: UNDER LARGE MAGNETIC POWER REGIME

Maycol Marcondes Vargas

Master Thesis at Post Graduation Course in Space Engineering and Technology/Combustion and Propulsion, guided by Dr. Fernando Fachini Filho, approved in February 26, 2014.

URL of the original document:

[<http://urlib.net/8JMKD3MGP5W34M/3FKEKF5>](http://urlib.net/8JMKD3MGP5W34M/3FKEKF5)

INPE
São José dos Campos
2014

PUBLISHED BY:

Instituto Nacional de Pesquisas Espaciais - INPE

Gabinete do Diretor (GB)

Serviço de Informação e Documentação (SID)

Caixa Postal 515 - CEP 12.245-970

São José dos Campos - SP - Brasil

Tel.:(012) 3208-6923/6921

Fax: (012) 3208-6919

E-mail: pubtc@sid.inpe.br

BOARD OF PUBLISHING AND PRESERVATION OF INPE INTELLECTUAL PRODUCTION (RE/DIR-204):**Chairperson:**

Marciana Leite Ribeiro - Serviço de Informação e Documentação (SID)

Members:

Dr. Antonio Fernando Bertachini de Almeida Prado - Coordenação Engenharia e Tecnologia Espacial (ETE)

Dr^a Inez Staciarini Batista - Coordenação Ciências Espaciais e Atmosféricas (CEA)

Dr. Gerald Jean Francis Banon - Coordenação Observação da Terra (OBT)

Dr. Germano de Souza Kienbaum - Centro de Tecnologias Especiais (CTE)

Dr. Manoel Alonso Gan - Centro de Previsão de Tempo e Estudos Climáticos (CPT)

Dr^a Maria do Carmo de Andrade Nono - Conselho de Pós-Graduação

Dr. Plínio Carlos Alvalá - Centro de Ciência do Sistema Terrestre (CST)

DIGITAL LIBRARY:

Dr. Gerald Jean Francis Banon - Coordenação de Observação da Terra (OBT)

DOCUMENT REVIEW:

Marciana Leite Ribeiro - Serviço de Informação e Documentação (SID)

Yolanda Ribeiro da Silva Souza - Serviço de Informação e Documentação (SID)

ELECTRONIC EDITING:

Maria Tereza Smith de Brito - Serviço de Informação e Documentação (SID)

Luciana Manacero - Serviço de Informação e Documentação (SID)



Ministério da
**Ciência, Tecnologia
e Inovação**



sid.inpe.br/mtc-m21b/2014/01.23.11.02-TDI

EFFECT OF TRANSIENT GAS-PHASE ON FERROFLUID DROPLET VAPORIZATION: UNDER LARGE MAGNETIC POWER REGIME

Maycol Marcondes Vargas

Master Thesis at Post Graduation Course in Space Engineering and Technology/Combustion and Propulsion, guided by Dr. Fernando Fachini Filho, approved in February 26, 2014.

URL of the original document:

[<http://urlib.net/8JMKD3MGP5W34M/3FKEKF5>](http://urlib.net/8JMKD3MGP5W34M/3FKEKF5)

INPE
São José dos Campos
2014

Cataloging in Publication Data

Vargas, Maycol Marcondes.

V426e Effect of transient gas-phase on ferrofluid droplet vaporization:
under large magnetic power regime / Maycol Marcondes Vargas.
– São José dos Campos : INPE, 2014.
xxii + 66 p. ; (sid.inpe.br/mtc-m21b/2014/01.23.11.02-TDI)

Thesis (Master in Space Engineering and Technology/Combustion and Propulsion) – Instituto Nacional de Pesquisas Espaciais, São José dos Campos, 2014.

Guiding : Dr. Fernando Fachini Filho.

1. droplet vaporization. 2. magnetic heating. 3. ferrofluid.
4. transient regime. I.Título.

CDU 536.423.1



Esta obra foi licenciada sob uma Licença [Creative Commons Atribuição-NãoComercial 3.0 Não Adaptada](#).

This work is licensed under a [Creative Commons Attribution-NonCommercial 3.0 Unported License](#).

Aprovado (a) pela Banca Examinadora
em cumprimento ao requisito exigido para
obtenção do Título de **Mestre** em

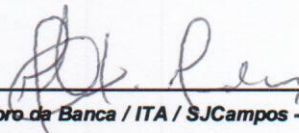
Engenharia e Tecnologia
Espaciais/Combustão e Propulsão

Dr. Fernando Fachini Filho



Presidente / Orientador(a) / INPE / Cachoeira Paulista - SP

Dr. Marcio Teixeira de Mendonça



Membro da Banca / ITA / SJCampos - SP

Dr. Wladimir Mattos da Costa Dourado



Membro da Banca / IAE/DCTA / São José dos Campos - SP

Dra. Elaine Maria Cardoso



Convidado(a) / UNESP / Ilha Solteira - SP

Dr. Cesar Flaubiano da Cruz Cristaldo



Convidado(a) / UNIPAMPA / Alegrete - RS

Este trabalho foi aprovado por:

() maioria simples

(x) unanimidade

Aluno (a): **Maycol Marcondes Vargas**

São José dos Campos, 26 de Fevereiro de 2014

“To know, is to know that you know nothing. That is the meaning of true knowledge.”.

SOCRATES

*A meus pais Francisco e Celi e a meus filhos Derick e
Drake*

ACKNOWLEDGEMENTS

I would like to express my gratitude to Dr. Cesar Flaubiano da Cruz Cristaldo for the support of my thesis study and research. I also would like to express my gratitude to my advisor Dr. Fernando Fachini Filho. His guidance helped me all the time in the research and writing of my thesis.

Besides them, I would like to thank CAPES who provided funding for my thesis.

Last but not the least, I would like to thank my family: my parents Francisco Rodrigues Vargas and Celi Marcondes Vargas, for supporting me all the time.

ABSTRACT

In this work the influence of transient processes of the gas phase on the vaporization of isolated ferrofluid droplet with spherical symmetry under the influence of an external alternating magnetic field is investigated. Dispersed magnetic nanoparticles inside the droplet act as a heat source. The nanoparticle dipole reacts to the alternating magnetic field rotating the nanoparticle. The friction between the rotating nanoparticle and the surrounding liquid produces heat (viscous dissipation). Brownian motion of the liquid molecules is responsible for the nanoparticle dipoles misalignment when the magnetic field amplitude is null. Therefore, in each cycle of the magnetic field the nanoparticle rotates, generating heating in the core of the liquid. Applying this process on droplets is possible to reduce the droplet heating time. The conditions addressed in this problem leads to the magnetic power to be much larger than the thermal power, provided by the heat flux from the gas phase. The characteristic of this problem is a thermal boundary layer established close to the droplet surface in the liquid side. The magneto relaxation source is found to be dependent on initial conditions. In addition, because of the dependency of the magneto relaxation heating on temperature, a local maximum of temperature is found inside the thermal boundary layer. In the current model it is also observed the increasing of the droplet vaporization with pressure.

EFEITO DA ETAPA TRANSIENTE DA FASE GASOSA NA VAPORIZAÇÃO DE UMA GOTA DE FERROFLUIDO: GRANDE POTÊNCIA MAGNÉTICA.

RESUMO

Neste trabalho é estudado a influência dos processos transientes da fase gasosa na vaporização de uma gota isolada de ferrofluido com simetria esférica e sob influência de um campo magnético externo alternado. Nanopartículas magnéticas homogeneamente dispersas no fluido agem como uma fonte de calor. Os dipolos das nanopartículas respondem ao campo magnético alternado fazendo a nanopartícula rotacionar. O atrito entre a nanopartícula e o líquido nos arredores da partícula produz calor (dissipação viscosa). O movimento Browniano das moléculas do líquido é responsável pelo desalinhamento dos dipolos na ausência do campo magnético. Desse modo em cada ciclo do campo magnético as nanopartículas rotacionam, gerando calor dentro da gota. Aplicando esse processo em gotas é possível reduzir o tempo de aquecimento. As condições assumidas neste problema resultam em uma potência magnética muito maior do que a potência térmica, dada pelo fluxo de calor da fase gasosa. A característica desse problema consiste em uma camada limite térmica estabelecida bem próximo à superfície no lado líquido da gota. O fonte magnética é dependente das condições iniciais do problema. Além disso, devido à dependência da fonte magnética com a temperatura, uma temperatura máxima local dentro da camada limite térmica é encontrada. O modelo atual observa o aumento da taxa de vaporização da gota com a pressão.

LIST OF FIGURES

	<u>Pág.</u>
2.1 Schematic representation of the current problem.	13
3.1 Schematic representation of temperature profile of the problem: (a) Liquid and gas phases is spatial coordinate r . (b) Liquid phase in spatial coordinate x and gas phase in spatial coordinate r	20
5.1 Temperature profile inside the droplet $p_m = 1.0$ and $f = 1.0$ for $T_\infty = 0.9$ ($T_\infty^* = 334.39$ K).	31
5.2 Temperature profile inside the droplet $p_m = 1.0$ and $f = 1.0$ for $T_\infty = 3.0$ ($T_\infty^* = 1114.65$ K).	32
5.3 Vaporization rate as a function of frequency for different ambient temperatures $T_\infty = 0.9$ ($T_\infty^* = 334.39$ K), $T_\infty = 3.0$ ($T_\infty^* = 1114.65$ K), $T_\infty = 6.0$ ($T_\infty^* = 2229.3$ K), for $p_m = 1.0$	33
5.4 Surface temperature as a function of frequency for different ambient temperatures $T_\infty = 0.9$ ($T_\infty^* = 334.39$ K), $T_\infty = 3.0$ ($T_\infty^* = 1114.65$ K), $T_\infty = 6.0$ ($T_\infty^* = 2229.3$ K), for $p_m = 1.0$	34
5.5 Heating time as a function of frequency for different ambient temperatures $T_\infty = 0.9$ ($T_\infty^* = 334.39$ K), $T_\infty = 3.0$ ($T_\infty^* = 1114.65$ K), $T_\infty = 6.0$ ($T_\infty^* = 2229.3$ K), for $p_m = 1.0$	35
5.6 Vaporization rate as a function of time for different p_m regimes, $T_\infty = 0.9$ ($T_\infty^* = 334.39$ K) and $f = 1.0$	36
5.7 Validation: vaporization rate as a function of time for pressure $P^* = 0.36$ atm and ambient temperature a) $T_\infty^* = 305$ K, b) 500 K, c) 1000 K corresponding to $p_m = 0.044, 0.027, 0.013$, respectively.	39
5.8 Temperature evolution for condition of $p_m = 0.0134$ ($T_\infty^* = 1000$ K, $P^* = 0.36$ atm) and $f = 1$	40
5.9 Heat flux in the droplet surface (a^-) as a function of time for the condition of $p_m = 0.0134$ ($T_\infty^* = 1000$ K, $P^* = 0.36$ atm) and $f = 1$	41
5.10 Temperature profile at heating time for different conditions of pressure and magnetic frequency: $P^* = 0.36$ and 25 atm; $f = 1$ and 5, with $k_{l\ ef}^*$ and k_l^* for $T_\infty^* = 1000$ K.	42
5.11 Droplet surface temperature as a function of time for different conditions ($T_\infty^* = 1000$ K, $P^* = 0.36$ and 25 atm; $f = 1$ and 5), considering $k_{l\ ef}^*$ and k_l^*	44

5.12	Vaporization rate as a function of time a) low (0.36 atm) and b)high (25.0 atm) pressure ($T_{\infty}^* = 1000$ K and $f = 1$ and 5), considering $k_{l\ ef}^*$ and k_l^*	45
5.13	Vaporization rate as a function of time for different pressure regime ($T_{\infty}^* = 1000$ K, $f = 1$)	46
5.14	Latent heat of vaporization and boiling temperature as a function of pressure ($T_{\infty}^* = 1000$ K, $f = 1$)	46

LIST OF SYMBOLS

a^*	–	Droplet radius - m
a_0^*	–	Initial droplet radius - m
a	–	Dimensionless droplet radius
a_0	–	Dimensionless initial droplet radius
\dot{a}	–	Time derivative of droplet radius - m/s
A	–	Dimensionless parameter - $c_p^* k_l^* / (c_l^* k_{g\infty}^*)$
c_l^*	–	Specific heat capacity at constant pressure of the liquid phase - J/gK
$c_{l\ ef}^*$	–	Effective specific heat capacity of the fluid - J/gK
c_n^*	–	Specific heat capacity at constant pressure of the nanoparticle - J/gK
c_p^*	–	Specific heat capacity at constant pressure of the gas phase - J/gK
f^*	–	Magnetic field frequency - Hz
f	–	Dimensionless frequency
H_0^*	–	Magnetic field amplitude - kA/m
$k_{g\infty}^*$	–	Thermal conductivity of the gaseous phase - W/mK
k_l^*	–	Thermal conductivity of the liquid phase - W/mK
$k_{l\ ef}^*$	–	Effective thermal conductivity of the fluid - W/mK
k_n^*	–	Thermal conductivity of the nanoparticle - W/mK
L^*	–	Latent heat of vaporization - J/g
L	–	Dimensionless heat of vaporization
Le_F	–	Vapor (n-Heptane) Lewis number
M_d^*	–	Domain magnetization - kA/m
M_F^*	–	Molecular weight of the fuel - g/mol
\dot{m}^*	–	Vaporization rate - kg/s
P^*	–	Pressure - atm or MPa
P_{crit}^*	–	Critical pressure - atm
P_m	–	Dimensionless parameter, ratio of magnetic power to thermal energy
p_m	–	Re-scaled dimensionless magnetic parameter - $p_m = P_m \varepsilon$
P_r	–	Reduced pressure - $P_r = P^* / P_{crit}$
r^*	–	Radial coordinate - m
r	–	Dimensionless radial coordinate
R_0^*	–	Universal gas constant - $J/(molK)$
t^*	–	Time - s
t	–	Dimensionless time
t_B^*	–	Brownian relaxation time - s
t_{Bb}^*	–	Effective relaxation time determined at the boiling temperature - s
t_h^*	–	Heating time - s
t_m^*	–	Effective relaxation time - s
t_N^*	–	Néel relaxation time - s
T^*	–	Temperature - K
T	–	Dimensionless temperature

T_b^*	– Boiling temperature - K
T_{crit}^*	– Critical temperature - K
T_r	– Reduced temperature - $T_r = T^*/T_{crit}$
T_s	– Dimensionless surface temperature
u^*	– Gas velocity - m/s
u	– Dimensionless gas velocity
x	– Coordinate used to spatially represent the thermal boundary layer
Y_F	– Fuel mass fraction
Y_{Fs}	– Fuel mass fraction at the surface, given by Clausius-Claperyon relation
Z_g	– Compressibility factor for the vapor
Z_l	– Compressibility factor for the liquid

Greek letters

(lowercase):

α_∞^*	– Thermal diffusivity - m^2/s
β	– Ratio of nanolayer thickness to the nanoparticle radius
γ	– Heat capacity ratio
δ	– Dimensionless boundary layer thickness
ε	– Gas-Liquid density ratio
λ	– Dimensionless vaporization rate
μ_0^*	– Magnetic permeability - H/m
ξ	– Langevin parameter
π	– Mathematical constant
$\rho_{l\ ef}^*$	– Liquid effective density - kg/m^3
ρ_n^*	– Nanoparticles density - kg/m^3
ρ_l^*	– Liquid density - kg/m^3
ρ_∞^*	– Gas density - kg/m^3
τ	– Dimensionless re-scaled time
τ_{hr}	– Dimensionless heating time reduction
ϕ	– Volume fraction of nanoparticles
χ	– Magnetic susceptibility

(uppercase):

ψ	– Coordinate used to represent the the gas phase
--------	--

Superscripts

–	– Region close to the droplet surface in the liquid side of the droplet
+	– Region close to the droplet surface in gaseous phase

CONTENTS

	<u>Pág.</u>
1 INTRODUCTION	1
1.1 Atomization	1
1.2 Isolated droplet	3
1.3 Slurry	6
1.4 Nanofluids	6
1.5 Ferrofluids	8
1.6 Objective	10
1.7 Work description	11
2 ANALYSIS	13
2.1 Characteristic times	13
3 MATHEMATICAL FORMULATION	17
3.1 Liquid Phase	17
3.2 Gas Phase	21
3.2.1 Stream function	22
4 NUMERICAL CODE	25
4.1 Numerical strategy	25
4.2 Discretization	25
4.2.1 Liquid Phase	26
4.2.2 Gas Phase	27
5 RESULTS	29
5.1 Constant property model	29
5.2 Variable property model	37
6 CONCLUSION AND FUTURE WORKS	49
6.1 Future works	49
REFERENCES	51
APPENDIX	59
A.1 Vaporization rate	59
A.2 Adimensionalization	59

A.2.1	Liquid phase	60
A.2.1.1	Mass conservation	60
A.2.1.2	Energy conservation	61
A.2.2	Gas phase	64
A.2.2.1	Mass conservation	64
A.2.2.2	Energy conservation	64
A.2.2.3	Species conservation	65

1 INTRODUCTION

Combustion of liquid fuels in sprays is the most common source of energy in use nowadays. Consequently burning of liquid fuels becomes one of the main pollutant source, making it a scientific and technological issue with direct environmental implications. These two facts are sufficient to justify huge effort in understanding their controlling processes. The goal of that is to achieve clean and efficient burning. Since spray combustion is controlled by phenomena in a large range of spatial (about five order of magnitude) and time scale (about four order of magnitude) its description is, without doubt, one of the most challenging task. In this section, the most important mechanisms of smallest and largest scales, i.e., heating, vaporization and combustion of isolated droplet and the liquid brake up into spray, respectively, are discussed.

1.1 Atomization

Since combustion occurs in the gas phase, except in some specific cases like gas-less flames and catalytic combustion ([MERZHANOV, 1997](#); [PFEFFERLE; PFEFFERLE, 1986](#)), liquid fuels must be vaporized before burning. To achieve vaporization rates high enough to provide high heat release in liquid combustion devices a large heat transfer to the liquid phase is necessary. This condition is found by breaking the liquid into very small droplets (atomization process). The atomization process is an intermediate step between a volume of liquid fuel and fuel vapor. That process is responsible for breaking the liquid fuel into a cloud with a huge number of small droplets.

The atomization process is the result of an imbalance among stabilizing forces, e.g., surface tension and viscosity, and destabilizing ones, e.g., aerodynamic and pressure ([LEFEBVRE, 2011](#)).

Atomization, which is one of the mechanisms of spray combustion, starts converting the liquid into a jet or liquid sheet. These configurations are very unstable to any geometric disturbance. The destabilizing forces make the disturbance amplitude to increase. The result is jet or liquid sheet breakup into ligaments. The same forces are responsible for breaking the ligaments into droplets. The diameter of the ligaments, which has a direct relation to the droplet diameters in the primary atomization, is a function of reciprocal of the jet or liquid sheet speed. Large droplets are still unstable and can suffer further atomization ([LEFEBVRE, 2011](#)).

Initially, liquid jet break up was studied taking into account a laminar flow through a circular orifice. It was assumed that the growth of small disturbances with certain wavelength is the beginning of the liquid breakup (RAYLEIGH, 1878). Later that analysis was extended, including the effects of air resistance and liquid viscosity in the jet disintegration (WEBER, 1931).

Devices used for atomizing liquids receive the name of atomizers, applicators, sprayers or nozzles. These devices use different methods for reaching the liquid atomization. The more common types share the same processes, which is discharging the liquid at high speeds into a quiescent gas, creating a high velocity gradient between them. Some improvements are made on the atomization process imposing angular velocity through a rotating cup and using an auxiliary air flow which causes extra disturbances in the fluid. Atomization is also performed by others mechanisms. By charging electrically the liquid with one polarity and charging the exit of the nozzle with the other polarity, the attractive force between them produces the liquid breakup into droplets. This mechanism is known as electrostatic atomization. In addition, forcing the liquid through a vibrating transducer, which imposes pressure disturbance with specific frequency and amplitude, causes the liquid brake up. This mechanism is known as ultrasonic atomization (LEFEBVRE, 2011).

In order to demonstrate the importance of the atomization process, a hypothetical case is proposed: to atomize a volume of 1 cm^3 of fuel which has a surface area of 4.836 cm^2 (sphere). The final state of this volume is a cloud of droplets with radius of $30 \mu\text{m}$, droplet size found in diesel engines (KOO; MARTIN, 1990). Then the cloud will be composed by about 8.8 million droplets with total surface area equal to 1000 cm^2 . The huge surface area will be responsible for the huge heat transfer from the gas phase to the liquid, process which controls the vaporization. Considering the thermal conductivity and the temperature gradient constant, the ratio of heat transfer for the two cases is

$$\frac{\bar{q}_c}{\bar{q}_s} = \frac{A_c k \bar{\nabla} T}{A_s k \bar{\nabla} T} \sim \frac{A_c}{A_s} = 207.8$$

The final area (area of the cloud of droplets A_c) is 207.8 times the initial surface area (area of a single droplet A_s). Then, it would be expected that the last fuel state would be vaporized about 207 times faster than the former fuel state, providing a power 207 times higher.

Once the liquid fuel is converted into a cloud of small droplets with a specific

droplet distribution of number density and velocity, the next step is to determine the vaporization rate of the spray. To achieve this goal, the description of the heating and vaporization of a single droplet becomes mandatory.

1.2 Isolated droplet

The study of a isolated droplet has two different aspects: the first one consists in understanding the transport phenomena and fluid dynamic of a heating and vaporizing droplet and the second aspect consists in developing models, which are able to describe them. Under some conditions an exact solution of the governing equations is found. Such models are necessary in spray combustion simulations because of its multi-scale (time and space) phenomena as already mentioned (SIRIGNANO, 1999; FACHINI, 2007).

Studies on droplet vaporization was first performed in 1938, when a correlation between momentum, heat and mass transfer for an evaporating single droplet was experimentally established (FRÖSSLING, 1938). Since then, a huge number of studies have been made in order to improve the accuracy and to generalize the correlation. In 1953, two systematic and detailed studies were performed in which the vaporization process was modeled considering a spherically symmetric pure-component isolated droplet burning in a quiescent oxidizing-gas phase. In a quiescent environment the flow is generated by the phase change during the vaporization (Stefan flow). Since the flow velocity is low compared to the sound velocity, isobaric processes were considered. Furthermore, since the thermal inertia of the gas phase surrounding the droplet is small compared to that one for the liquid phase, the quasi-steady condition is assumed for the gas phase close to the droplet. Under these conditions, the evolution of the square of the droplet radius was found to decrease linearly with time, known D^2 -law (SPALDING, 1953; GODSAVE, 1953). Further studies were performed extending the problem by using a linear temperature dependency for the thermal conductivity and heat capacity (GOLDSMITH; PENNER, 1954). Experimentally, it was proved that the quasi-steady combustion model is still valid for bigger droplets (6000μ) (WISE H., 1955). Besides, by using the Burke-Schumann hypothesis (BURKE; SCHUMANN, 1928), the flame position of a non-premixed configuration is where stoichiometry is found. In addition, another important result was observed: the droplet burning rate is proportional to the droplet radius and the flame is always at the same position in relation to the droplet surface (OZAKI; GOMI, 1953). From experimental studies, it is shown that the relation between the mass burning rate

to the droplet radius is valid for a wide range of experimental conditions, even for droplet radius of about 1 mm with normal gravitational field (GOLDSMITH; PENNER, 1954; KOBAYASHI, 1954).

Once the fuel droplet size treated in the current work is micron-sized (smaller by two orders of magnitude in comparison with the previous works) the gravity influence is still smaller, therefore it can be neglected.

There are also complementary works, reviewing the single droplet combustion history extending the discussion to future applications. In these works, single droplet combustion cases, stationary and moving droplets are considered, taking into account the influence of high ambient temperature, pressure and ignition (WILLIAMS, 1973; FAETH, 1977; SIRIGNANO, 1983).

There are several models for describing the liquid phase of the vaporizing-droplet problem. Each model considers a group of conditions, which justify its use for specific situations. When the fluid is very low volatile, the heating time can be considered separated from the vaporization rate. Then the vaporization occurs at droplet temperatures practically the same as the boiling temperature. When the droplet has relative velocity with the gas phase, the shear between the phases generates recirculation inside the droplet. Consequently, the temperature profile of the droplet can be considered uniform. This same feature is achieved when the thermal conductivity is large. Then this model is used for droplet description with relative velocity (SIRIGNANO, 1999).

When the relative velocity is not large, the time and space dependence of the temperature profile inside the droplet is evident. In this situation, the whole thermal problem must be considered in the description of the droplet problem.

In the description of the gas phase of a vaporizing-droplet problem, three assumptions are available: steady-state, quasi-steady state and transient.

In the single droplet context, steady state condition is achieved under the assumption of a vaporizing droplet without time dependent variables, such as: radius, vaporization rate, and temperature. Such regime is commonly validated by use of a porous sphere, in which by supplying with liquid at the same rate as it is vaporized, after a transient period (droplet heating) a steady regime is established (MARCHESE; DRYER, 1996; SAMI; OGASAWARA, 1970).

Imposing the quasi-steady assumption, the transient term is removed from the gov-

erning equations, and the time dependence is on the droplet heating and vaporization process. For each time step, the flow field is considered to be completely developed to the conditions at the droplet surface. That assumption is justified for low pressure regime and only close to the droplet, at distances of order of the droplet radius. However, regions far from the droplet surface the quasi-steady assumption does not prevail. Considering the ratio of the gas phase density to the liquid phase density denoted by ε , the region in which the transport phenomena are transient is estimated by the square root of reciprocal of that ratio, $\varepsilon^{-1/2}$. For atmospheric conditions $\varepsilon \sim 10^{-3}$, then the transient processes are at a distance from the droplet of about $30a$, a is the droplet radius (CRESPO; LINÀN, 1975; WALDMAN, 1975; FACHINI et al., 1999).

For the droplet vaporization and burning under high pressure regime, the thermal inertia of the gas phase approximates to that of the liquid phase. The gas phase close to the droplet loses its quasi-steady characteristics and transient treatment becomes necessary. At the thermodynamic critical condition, the gas - liquid density ratio becomes of order unit.

An experimental study on the combustion of droplets without influence of gravity, showed that the heat and mass transfer outside the flame cannot be well predicted by considering the quasi-steady model (ISODA; KUMAGAI, 1958).

It is possible to say that description of the heating, vaporization and burning of a droplet requires indispensably the inclusion of the transient (mass and energy accumulation) process together with convection and diffusion processes (FACHINI, 2007). Also, at high pressure regime some processes, negligible at low pressure regime, must be included in the description of droplet problem, e.g., solubility of gases into the droplet and the effects of real gas in the liquid-gas equilibrium condition at the interface (JIA; GOGOS, 1994).

The heat transfer from the gas phase to the liquid phase is the controlling process of the heating and vaporization of liquid fuels. Then the atomization process is crucial because of the huge surface area of the cloud of droplets. Other factors improve the heating and vaporization processes but not compared to the atomization. One of them is the change on the thermal conductivity of the liquid fuels with a mixture with other fuels, but the change is marginal. Another way of increasing substantially the thermal conductivity is to mix fuels with micrometer- or millimeter-sized solid particles.

1.3 Slurry

These millimeter-sized solid particles seeded into fluids are denominated slurries (SZEKELY, 1981). Slurries can present liquid phase composed of water, oil, fuel, while the solid inert/reacting particles can be of metals, biomass, coal or any material of interest. In some combustion cases, the addition of the solid particles can lower the consumption of fuel and lower CO emission. (PRAKASH; SHANKAPAL, 2007).

Slurries are more advantageous than pure fuels, in terms of combustion efficiency. But such fluids present problems as sedimentation of the particles, abrasive action and obstruction of small channels which forbid its commercial usage (DAS et al., 2003). Solution for these previous problems can be obtained by reducing the particle sizes, but it will be better explained ahead.

Since Maxwell's theoretical work has been published (MAXWELL, 1881), several theoretical and experimental studies has been performed on the area of these hybrid fluids. But due to the large sized-particles and high density of the particles, there is not a good way to prevent these solid particles to settle down. The very low stability of the slurries is also a major problem. But modern technology presents processes capable of producing particles with average size of 10 nm which can be seeded in fluids. This colloidal solution of solid and liquid is defined as nanofluids and is much more stable.

1.4 Nanofluids

Nanofluids are fluids consisting of liquid carriers containing stable dispersed surface-coated nanoparticles of about 10 nm. The term nanofluid was proposed by Choi (CHOI, 1995). Recently this kind of fluid has become the focus of research. The increase of interest in the nanofluid area can be measured by the number of analysis published in the last decade: in 2000, 12 articles were published, against 78 in 2005 and almost 500 in 2010 (TAYLOR et al., 2012). Due to the increase in the use of this kind of fluid, a good understanding of their modeling and properties are necessary.

The suspension of solid particles into liquid has long been recognized to have a huge potential as enhanced heat-management fluid. Nanofluids due to the high thermal conductivity of its solid particles, will have higher thermal conductivity when compared with pure fuels. It makes nanofluids a better heat exchanger, which is the advantage of such fluids (KEBLINSKI et al., 2002). The enhancement caused by the

addition of nanoparticles into liquid becomes evident with a example. Adding 0.3% volume fraction of 10 nm Cu nanoparticles, an increase of about 40% was found in the thermal conductivity of ethylene glycol (EASTMAN et al., 2001). That result is one order of magnitude larger than the one predicted by the macroscopic theory (KEBLINSKI et al., 2002).

Nanofluid particles (nanoparticles) are under constant interaction with liquid (collisions due Brownian motion), which is strongly dependent on van der Waals force. The collisions among the nanoparticles undesirably lead to the agglomeration of such particles, generating large-sized particles. These bigger and consequently heavier particles are unable to be maintained in suspension by Brownian motion and tend to settle down (same problem of slurries). The use of coating-layers (surfactant) is a common way to prevent that. Even with advantages, nowadays, the usage of nanofluids are still limited, e.g., the deterioration of the surfactant at moderate/low temperatures restrains the use of nanofluids in combustion problems. New studies are required on those applications to use nanofluids commercially (TAYLOR et al., 2012; GHADIMI AND R. SAIDUR, 2011).

The typical understanding of the effective thermal conductivity of nanofluids has its basis on continuum formulations, which generally account for only the particle shape or size and volume fraction, assuming diffusive heat transfer in both phases (liquid and solid). But until now, complete understanding of the unusual heat transfer characteristics of nanofluids has not been reached (WANG; MUJUMDAR, 2007). Several mechanisms, such as: Brownian motion of the nanoparticles, interfacial ordering of liquid molecules on the surface of nanoparticles, ballistic transport of energy inside individual nanoparticles and between nanoparticles that are in contact, and also, nanoparticles structure/networking, have been proposed for describing the experimentally observed huge thermal conduction enhancement (KEBLINSKI et al., 2002; WANG et al., 2003; YU; CHOI, 2003; PATEL et al., 2003; KUMAR et al., 2004; SHENOGIN et al., 2004a; SHENOGIN et al., 2004b; PRASHER et al., 2006). Much has been debated in the past few years, and the focus of the debate has been on the role of Brownian motion (KUMAR et al., 2004; KOO; KLEINSTREUER, 2005; KEBLINSKI; CAHILL, 2005; EVANS et al., 2006) and interfacial ordering (YU; CHOI, 2003; SHENOGIN et al., 2004a; SHENOGIN et al., 2004b; PRASHER et al., 2005). In the work of (DING et al., 2007), much is discussed about the dominant mechanism. The discussion indicates that Brownian motion, liquid layering and ballistic transport of energy in nanofluids cannot be the dominant mechanism. Leaving space for, as the authors call, the 'last standing mechanism': nanoparticle structure/networking (PRASHER et al., 2006; KEBLINSKI,

2007). This is validated by experimental and theoretical analysis of ethylene-glycol-based titania nanofluids (PRASHER et al., 2006). In that work is found that the size of the aggregates is approximately 3.5 times the initial nanoparticles. Through use of Maxwell model for aggregate suspensions and Bruggeman model for aggregates, a nanoparticle structuring model is formulated, showing a good agreement with experimental data (CHEN et al., 2007). Still, no general method for accurately predicting this anomalous thermal conductivity enhancement is available.

Applications for this kind of fluid can be found from biomedical, diagnosis, treatment of diseases, to technological ones. In medicine, nanofluids are referred to as nano-scale colloidal solutions. In that area, these fluids are largely studied in cancer treatment and optofluid control of fluid motion (TAYLOR et al., 2012). As an technological example, the use of Al_2O_3 particles with average-sized particles of 13 nm in diameter into water can be mentioned. A volume fraction of 4.3% of particles enhanced the thermal conductivity of water under stationary conditions in 30% (MASUDA et al., 1993). By using the same configuration of the previous example but with bigger-sized particles (40 nm average) the increase was of 10% (LEE et al., 1999).

These fluids, as cited before, have high thermal conductivity in comparison with pure fuels, hence it can present several benefits in working with.

An experiment of dropping a reacting nanofluid in a hot-plate, shows that the ignition probability of the droplet is higher in nanofluids than in pure fuels (TYAGI et al., 2008). Also anomalous thermal enhancement has been found by the addition of small quantities of copper nanoparticles, carbon nanotubes and magnetite nanoparticles and others colloidal nanoparticles into the fluid (EASTMAN et al., 2001; CHOI et al., 2001; KEBLINSKI et al., 2008; SHIMA et al., 2009; TYAGI et al., 2008; YETTER et al., 2009; PHILIP et al., 2007). A more complete list of nanofluids applications can be found (WONG; LEON, 2010). In addition, in the previous work, the role played by nanofluids are exhibited for the actual scenario and also its growing importance for the future.

1.5 Ferrofluids

Seeding a liquid with magnetic nanoparticles, magnetic properties are added to the nanofluids. This kind of nanofluids are known as ferrofluids. Ferrofluid is a colloidal suspension composed of magnetic nanoparticles, dispersed in a liquid carrier (PAPELL, 1965; OFFICE OF ADVANCED RESEARCH AND TECHNOLOGY, NATIONAL

AERONAUTICS AND SPACE ADMINISTRATION, 1967; ROSENSWEIG, 1985). The magnetic characteristic of ferrofluids enables the control of the fluid properties by frequency, amplitude and direction of external magnetic field. Also, in ferrofluids the magnetic particles are covered with a layer of dispersant in order to prevent the agglomeration of the particles, while thermal vibration of the particles/fluid molecules maintains the particles suspended in the fluid (Brownian motion). The size of particles is used to classify the fluid into two types: ferrofluids (particles diameter are nano-sized) and magneto-rheological (particles diameter are micron-sized) (PEREZ-CASTILLEJOS et al., 2000).

Magneto relaxation heating is the process responsible for transferring the energy absorbed from the magnetic field into heat. That process is controlled by relaxation mechanisms (ROSENSWEIG, 2002).

Magnetic nanoparticles dispersed into a liquid can be influenced by an external magnetic field. Each magnetic nanoparticle has a dipole which tends to align with the applied external magnetic field (ROSENSWEIG, 1985). When the magnetic field is null, Brownian motion of the fluid molecules causes the misalignment of the dipoles. Applying an alternate magnetic field to the ferrofluid, the magnetic nanoparticles rotate themselves in each cycle, generating heat by friction between the magnetic nanoparticle and the fluid (magneto Brownian relaxation source). There is another heating mechanism known as Néel mechanism. In this mechanism the nanoparticle dipole rotates while the nanoparticle remains static. The dipole rotation occurs within the crystal structure of the nanoparticle. It is responsible for increasing the nanoparticle temperature. The Néel mechanism is only significant at high frequencies. In the current work, the external magnetic field period is chosen to be of the order of the droplet heating time, under such configuration, the frequencies are far below the range in which the Néel mechanism present significant influence.

In the mid of 60's, ferrofluids were utilized to control flow of fuel in microgravity conditions (RAJ K., 1990). Today its use is not limited to that situation. One of the features regarding to ferrofluids is the ample applicability of such materials when compared to nanofluids. In 1965, non-stable suspensions containing magnetic particles were first synthesized (PAPELL, 1965) and have been extensively studied since then. In medicine, ferrofluids are used in experimental cancer treatment, where the tumor cells are filled with magnetic nanoparticles carried by ferrofluid, then under an external alternating magnetic field the cancerous cells are heated and destroyed (JORDAN AND REGINA SCHOLZ, 1999; KAPPIYOOR R., 2010). In technological area

ferrofluids application can be used as, for example: dynamic sealing and heat dissipation. A good example of dynamic sealing is hard disks of a computer, which has to operate in hermetically closed box to avoid the entrance of impurity. The sealing is made by making a hole inside a magnet and the shaft made of soft material. A groove in the shaft is filled with ferrofluid, which will be kept there due to the magnetic field blocking the passage of any impurity, sealing the axle and letting it free to rotate because of the obstructing material is ferrofluid. As a heat dissipator, ferrofluid fits due to two factors: the first one is its high thermal conductivity (good heat exchanger), the second one is that its magnetic properties can be used to maintain the ferrofluid in the place which needs cooling, i.e., in places where non magnetic liquid would flow away. An example for that is the loudspeaker. The loudspeaker coil heats up and the ferrofluid is kept in its place due to the magnetic field of the magnet fixed on the horn of the loudspeaker. Others examples are available in the literature (SCHERER; NETO, 2005). In recent studies, ferrofluids have been used to decrease the heating time of a vaporizing droplet (FACHINI; BAKUZIS, 2010; CRISTALDO; FACHINI, 2013a; CRISTALDO; FACHINI, 2013b). In the first work (FACHINI; BAKUZIS, 2010) a theoretical analysis is performed in the decreasing of heating time of a droplet under an alternated magnetic field. Analytical solutions are found for the liquid phase, the system is governed by Brownian and/or low-barrier Néel relaxation. A single droplet in an quiescent quasi-steady atmosphere is studied in the other two works (CRISTALDO; FACHINI, 2013a; CRISTALDO; FACHINI, 2013b). The results pointed out that magnetic energy source causes a uniform heating inside of the droplet. The heat flux provided by the environment only alters the temperature in a thin region close to the droplet surface (thermal boundary layer). Also, higher vaporization rates are observed (CRISTALDO; FACHINI, 2013a; CRISTALDO; FACHINI, 2013b).

The current study is an extension of these previous works. The consideration of the previous works are assumed in this work. As an extension work two differences are presented: the first is that no analytical solution is used in the liquid phase, the second is that the analysis is performed concerning about the transient effects of the gas phase on the droplet heating and vaporization of the droplet.

1.6 Objective

The objective of this study is to consider the transient processes in the gas phase on the vaporization of a ferrofluid droplet in a quiescent ambient under the influence of an external alternating magnetic field.

1.7 Work description

In this work, differently from the classical droplet problems in which heating and vaporization are dependent only on the heat from the gas phase, the droplet heating and vaporization of a single droplet are enhanced by the magneto relaxation source. As already mentioned, the magnetic particles respond to an external alternated magnetic field imposing the magneto relaxation heating inside the droplet (FACHINI; BAKUZIS, 2010; CRISTALDO; FACHINI, 2013a; CRISTALDO; FACHINI, 2013b). This process occurs due to the nanoparticle dipole alignment with the magnetic field, inducing the rotation of the nanoparticle. This movement occurs against the molecular forces, and the result is heat generation by friction (viscous dissipation). The condition addressed in the current analysis leads to the magnetic power much larger than the thermal power provided by the heat flux from the gas phase to the liquid phase (FACHINI; BAKUZIS, 2010; CRISTALDO; FACHINI, 2013a; CRISTALDO; FACHINI, 2013b). Under such regime, the transient accumulation of mass and energy in the gas phase close to the droplet become important even for low pressure conditions. To measure the influence of the transient processes on the heating and vaporization of ferrofluid droplets, the ambient pressure is chosen from sub-atmospheric conditions up to close to the critical condition.

2 ANALYSIS

The problem configuration consists of a single ferrofluid fuel droplet being heated by the heat flux provided by the gas phase and the magneto relaxation source. The droplet is in a quiescent atmosphere. Spherical symmetry is found, permitting to treat the problem as one dimensional. The droplet problem is divided in two domains: liquid and gas. A set of conservation equations are used to describe each one. Initially, the droplet has a radius $a^*(0) = a_0^*$ and temperature T_0^* . The liquid density ρ_l^* , the specific heat c_l^* and the thermal conductivity k_l^* are constants. The gas phase, far from the droplet, is composed by a mixture of air and fuel vapor $Y_{F\infty}^*$, with temperature T_∞^* , density ρ_∞^* , specific heat capacity c_p^* and thermal conductivity $k_{g\infty}^*$ which are constant. Lewis number in the gas phase is equal to unity and heat transfer by radiation is neglected.

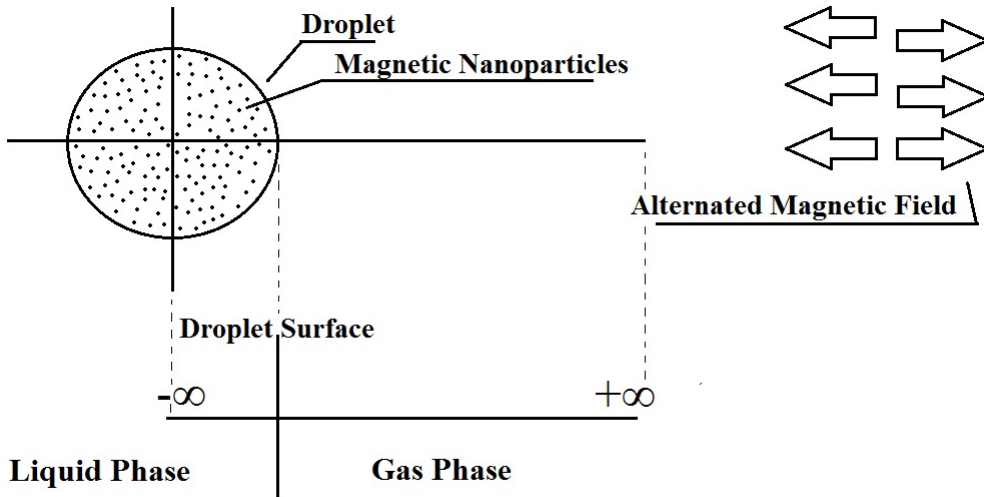


Figure 2.1 - Schematic representation of the current problem.

2.1 Characteristic times

In order to re-scale properly the problem, the most significant characteristic times must be determined. In this case, the heating and vaporization times will be evaluated (estimated).

To estimate the droplet heating time, it is assumed that all the heat transferred from the ambient to the droplet is used only to heat up the droplet. The droplet

temperature is determined by

$$\frac{\partial}{\partial t^*}(\rho_l^* c_l^* T^*) = \frac{1}{r^{*2}} \frac{\partial}{\partial r^*} \left[r^{*2} k_l^* \frac{\partial T^*}{\partial r^*} \right] \quad (2.1)$$

Assuming liquid thermal conductivity $k_l^* \gg 1$, then temperature is only dependent on time $T(t)$. Integrating the previous equation from the surface to its core results in

$$\rho_l^* c_l^* \frac{\partial}{\partial t^*} \left(T^* \frac{a^{*3}}{3} \right) = a^{*2} k_l^* \frac{\partial T^*}{\partial r^*} \Big|_{r=a^-}$$

As the heating process occurs without vaporization, the droplet radius a^* is constant. From the energy conservation at the droplet surface $k_l^* \nabla T|_{a^-} = k_g^* \nabla T|_{a^+}$.

$$\frac{\rho_l^* c_l^* a^{*3}}{3} \frac{dT^*}{dt^*} = a^{*2} k_g^* \frac{\partial T^*}{\partial r^*} \Big|_{r=a^+}$$

the following approximations are used $dT^* \sim \Delta T^* = T_b^* - T_0^*$, $dt^* \sim \Delta t^* = t_h^*$, $\partial T^* \sim \Delta T^* = T_\infty^* - T_b^*$ and $\partial r^* \sim \Delta r^* = a_0^*$ in which T_b^* is the liquid boiling temperature, then

$$\frac{\rho_l^* c_l^* a_0^{*3}}{3} \frac{(T_b^* - T_0^*)}{t_h^*} \sim a_0^* k_g^* (T_\infty^* - T_b^*)$$

leading to

$$t_h^* \sim \frac{1}{3} \frac{\rho_l^* c_l^*}{\rho_\infty^* c_p^*} \frac{(T_b^* - T_0^*)}{(T_\infty^* - T_b^*)} \frac{a_0^{*2}}{\alpha_\infty^*} \quad (2.2)$$

in which $\alpha_\infty^* = k_g^*/(c_p^* \rho_\infty^*)$ is the thermal diffusivity. Assuming $c_l^*(T_b^* - T_0^*)/[3c_p^*(T_\infty^* - T_b^*)] \sim 1$, the characteristic heating time can be estimated as

$$t_h^* \sim \frac{1}{\varepsilon} \frac{a_0^{*2}}{\alpha_\infty^*} \quad (2.3)$$

in which $\varepsilon \equiv \rho_\infty^*/\rho_l^*$.

Following the same procedure used for the estimation of characteristic heating time, an estimation for the vaporization time is determined. Under the assumption that the heat transferred to the droplet is now used to vaporize it, then the energy balance for the liquid is

$$-\frac{d}{dt^*} \left(4\pi\rho_l^* L \frac{a^{*3}}{3} \right) = \left[4\pi a^{*2} k_g^* \frac{\partial T^*}{\partial r^*} \right] \Big|_{r=a^+} \quad (2.4)$$

in which L is the latent heat of vaporization. Using the approximations $\partial T^* \sim \Delta T^* = T_\infty^* - T_b^*$, $\partial r^* \sim a_0^*$, $da^{*3} \sim a_0^{*3}$ on Eq. (2.4)

$$\frac{4\pi\rho_l^* L a_0^{*3}}{3} \frac{1}{t_v} \sim 4\pi a_0^{*2} k_g^* (T_\infty^* - T_b^*)$$

leading to

$$t_v \sim \frac{4\pi}{3} \frac{\rho_l^*}{\rho_\infty^*} \frac{L}{c_p^* (T_\infty^* - T_b^*)} \frac{a_0^{*2}}{\alpha_\infty^*}$$

Assuming $4\pi L/[3c_p^* (T_\infty^* - T_b^*)] \sim 1$, then

$$t_v \sim \frac{1}{\varepsilon} \frac{a_0^{*2}}{\alpha_\infty^*} \quad (2.5)$$

in which $\varepsilon \equiv \rho_\infty^*/\rho_l^*$. It is seen from Eqs. (2.3) and (2.5) that heating and vaporization time have the same order of magnitude. These estimations show that the problem will be well described by either heating or vaporization time.

There is another characteristic time in the droplet problem, that one describing the process in the gas phase, $t_g^* = a_0^{*2}/\alpha_\infty^*$. Therefore, the characteristic times related to the liquid phase $t_l^* = t_{h \text{ or } v}^* = a_0^{*2}/(\varepsilon\alpha_\infty^*)$ can be written as a function of the gas phase characteristic time, $t_l^* = t_g^*/\varepsilon$. At atmospheric conditions (normal conditions) $1/\varepsilon \sim 1000$, meaning a heating or vaporization time one thousand times longer than the characteristic time scale for the gas phase. Any disturbance at the droplet surface the gas phase will adapt almost instantaneously compared to the liquid phase. Therefore, under such condition, quasi-steady regime can be employed. Once,

there is a change in the density ratio variable ε , the thermal inertia of the gaseous phase changes. Any increase in ε means a increase in the response time of the gas phase (t_g^* approaches t_l^*), thus the transient treatment of gas phase becomes necessary when $\varepsilon \sim O(1)$.

3 MATHEMATICAL FORMULATION

The following dimensionless independent variables

$$r \equiv r^*/a_0^*, \quad t \equiv t^*/t_h^*$$

and dependent variables

$$a \equiv a^*/a_0^*, \quad T \equiv T^*/T_b^*, \quad u \equiv u^*/(\alpha_\infty^*/a_0^*), \quad \rho \equiv \rho^*/\rho_\infty^*, \quad Y_F \equiv Y_F^*/Y_{F\infty}^*$$

are used in the conservation equations. The variable r is the radial coordinate, t is the time, a is the droplet radius, T is the temperature, u is the gas velocity, ρ is the density and Y_F is the fuel mass fraction. The dimensional variables are denoted by the superscript $*$ whereas the subscripts b and ∞ represent the boiling and ambient conditions, respectively. The nondimensionalization of the equations are described at Appendix (A.2).

3.1 Liquid Phase

To describe the liquid phase, the dimensionless conservation equation of mass and energy are (FACHINI; BAKUZIS, 2010; CRISTALDO; FACHINI, 2013a; CRISTALDO; FACHINI, 2013b):

$$\frac{da^3}{dt} = -3\lambda \tag{3.1}$$

and

$$\frac{\partial T}{\partial t} - \frac{A}{r^2} \frac{\partial}{\partial r} \left(r^2 \frac{\partial T}{\partial r} \right) = P_m \frac{f^2 \tau_r(T)}{1 + [f \tau_r(T)]^2} \tag{3.2}$$

with the following boundary conditions:

$$\frac{\partial T}{\partial r} = 0, \quad \text{for } x \rightarrow -\infty \tag{3.3}$$

$$r^2 T^n \frac{\partial T}{\partial r} \Big|_{a^+} = \lambda L + r^2 A \frac{\partial T}{\partial r} \Big|_{a^-} \tag{3.4}$$

$\lambda(t) \equiv \dot{m}^*(t^*)c_p^*/(4\pi k_{g\infty}^*)$ is the dimensionless vaporization rate, $\dot{m}(t^*)$ is the dimensional vaporization rate, $A \equiv c_p^*k_l^*/c_l^*k_{g\infty}^*$ is a constant and $\tau_r \equiv t_h^*/t_{Bb}^*$ is the dimensionless magneto relaxation time. The right hand side of Eq. (3.2) represents the energy dissipation due to the rotation of the magnetic nanoparticles (magneto relaxation source) under the influence of an external alternate magnetic field. Equations (3.3) and (3.4) are the symmetry condition imposed at the droplet center and the heat conservation at the droplet surface, respectively.

The gas thermal conductivity is considered a function of the temperature according to $k_g^*/k_{g\infty}^* = T^n$, with $n = 0.5$. The dimensionless latent heat of vaporization is defined as $L \equiv L^*/(c_p^*T_b^*)$. The subscript a^- represents a region at the droplet surface in the liquid side, while a^+ represents a region at the surface in the gas side.

The dissipation of energy of the nanoparticles is provided by two mechanisms: viscous dissipation due to the rotation of the whole magnetic particle (the nanoparticle rotates along with its magnetic dipole) in a surrounding liquid (Brownian mechanism) and the augment of temperature of the nanoparticle rotation of the magnetic dipole within the nanoparticle (the nanoparticle does not rotate) (Néel mechanism). The most important parameter that determines the magnetic nanoparticles heating rate is the effective relaxation time (the characteristic time of misalignment of the dipole) defined as $t_r^{*-1} = t_B^{*-1} + t_N^{*-1}$, in which t_B^{*-1} is the Brownian relaxation time and t_N^{*-1} is the Néel relaxation time. Thus, the shorter relaxation time determines the dominating relaxation mechanism. The relaxation times depend on temperature T^* , in which $t_B^*(T^*) \equiv 3\eta V_H^*/(\kappa T^*)$ and $t_N^*(T^*) = \tau_0 \exp(\Gamma)[\pi/(4\Gamma)]^{1/2}$ (ROSENSWEIG, 1985). The parameter Γ is a temperature dependent function given by $\Gamma \equiv KV_N^*/(\kappa T^*)$, in which K is the anisotropy constant, V_N^* is the volume of magnetic nanoparticle, κ is the Boltzmann constant, τ_0 is the average relaxation time in response to a thermal fluctuation and η is the viscosity of the medium.

In this work, the condition $t_B^{*-1} \gg t_N^{*-1}$, is assumed, because the relaxation occurs mainly due to the Brownian mechanism, then $t_r^* = t_B^*$ (FACHINI; BAKUZIS, 2010). The Brownian relaxation time t_B^* is nondimensionalized by its value at the boiling temperature leading to $t_B \equiv t_B^*/t_{Bb}^* = 1/T$ (FACHINI; BAKUZIS, 2010).

The parameter P_m is the ratio of magnetic heat source to the thermal energy flux (provided by the gas phase), and it is described as:

$$P_m \equiv \frac{\mu_0^* \chi_0 H_0^{*2}}{2\rho_l^* c_l^* T_b^*} \frac{t_h^*}{t_{Bb}^*} \quad (3.5)$$

in which μ_0^* is the magnetic permeability, H_0^* is the magnetic field amplitude and χ_0 is the initial susceptibility described by the Langevin equation (FACHINI; BAKUZIS, 2010; CRISTALDO; FACHINI, 2013a; CRISTALDO; FACHINI, 2013b)

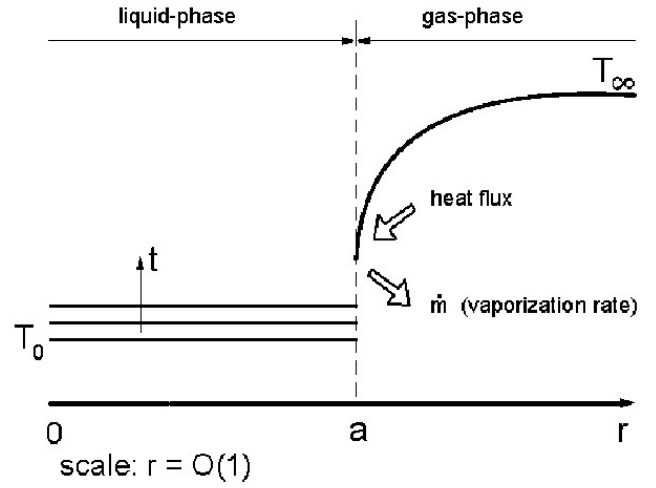
$$\chi_0 = \chi_i \frac{3}{\xi} \left(\coth \xi - \frac{1}{\xi} \right) \quad (3.6)$$

The initial susceptibility is described by $\chi_i \equiv \mu_0^* \Phi M_d^{*2} V_N^* / (3\kappa T^*)$, in which Φ is the volume fraction of nanoparticle and M_d^* is the domain magnetization. The Langevin parameter ξ is defined as $\xi = \mu_0^* M_d^* H^* V_n^* / (\kappa T^*)$, in which $H^* = H_0^* \cos(2\pi f^* t^*)$. Equilibrium susceptibility χ_0 is a conservative estimative for low limit of the source term in Eq. (3.2), then it can be assumed constant (ROSENSWEIG, 1985). That is possible because of the assumption of no variation in the volume fraction (very low radius variation).

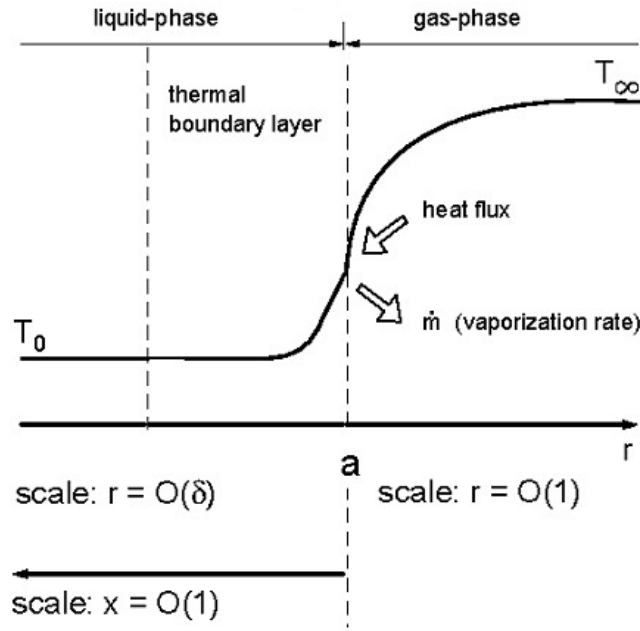
As observed in Eq. (3.2), the magnetic energy dissipation inside the droplet is controlled by two main parameters, the magnetic parameter P_m and the field frequency $f \equiv 2\pi f^* t_{Bb}^*$, in which f^* is the dimensional frequency, and t_{Bb}^* is the effective relaxation time determined at the boiling temperature.

The assumption of a very high magnetic parameter is used in this work, $P_m \gg 1$, implying in first approximation a uniform temperature profile inside the droplet, according to Eq. (3.2) (FACHINI; BAKUZIS, 2010). That assumption is valid for a field intensity of about 10^{-2} Tesla. Under this condition, the temperature profile is uniform in the droplet core, varying only with time Fig.3.1(a) (FACHINI; BAKUZIS, 2010). But, in a thin zone adjacent to the surface of the droplet the temperature profile, which is constant in the droplet core, changes to a time-spatial variation in order to match the temperature gradient imposed by the heat flux of the gas phase Fig. 3.1(b). As a consequence, a thermal boundary layer must be established adjacent to the droplet surface to describe properly the temperature profile (CRISTALDO; FACHINI, 2013a; CRISTALDO; FACHINI, 2013b). Figure 3.1 is taken from (CRISTALDO; FACHINI, 2013b).

For matching the liquid phase temperature with that of the gas phase, the temporal and spatial coordinates must be re-scaled. In new variables, the evolution of temperature inside the thermal boundary layer is well described. By analyzing Eq. (3.2), the appropriate time scale is $t \sim 1/P_m$, then the new time is $\tau \equiv t P_m$, for $\tau = O(1)$. The spatial coordinate is re-scaled according to $r = a + \delta x$. According to classical



(a)



(b)

Figure 3.1 - Schematic representation of temperature profile of the problem: (a) Liquid and gas phases in spatial coordinate r . (b) Liquid phase in spatial coordinate x and gas phase in spatial coordinate r .

procedure, the thermal boundary layer is established in the thickness δ , which is described by $x = O(1)$, as seen in Fig. 3.1(b). After the transformation, the system of Eqs. (3.1) to (3.4) becomes

$$\frac{da^3}{d\tau} = -3\frac{\lambda}{P_m} \quad (3.7)$$

$$\frac{\partial T}{\partial \tau} + \frac{1}{\delta} \frac{da}{d\tau} \frac{\partial T}{\partial \tau x} - \frac{A}{\delta^2 P_m} \frac{\partial^2 T}{\partial x^2} = \frac{f^2 T}{T^2 + f^2} \quad (3.8)$$

By making an asymptotic analysis on the source term $S(T, f) \equiv (f^2 T)/(T^2 + f^2)$ of Eq. (3.8), it is possible to observe that $S(T, f) \sim f^2/T \ll 1$ for low frequencies ($f \ll 1$) and $S(T, f) \sim T$ for high frequencies ($f \gg 1$). By doing $\delta = (A/P_m)^{1/2}$, all the terms of Eq. (3.8) become of $O(1)$, except the convective term that presents $O[(A/P_m)^{1/2}] \ll 1$ due to $da/d\tau \sim 1/P_m$ for low radius variation $a \sim 1$. Then the effects of the convection term due to the low variation of radius is negligible whereas $a \gg P_m^{-1/2}$. Therefore imposing $\delta = (A/P_m)^{1/2}$, Eq. (3.8) becomes

$$\frac{\partial T}{\partial \tau} = \frac{\partial^2 T}{\partial x^2} + \frac{f^2 T}{T^2 + f^2} \quad (3.9)$$

with the boundary conditions:

$$\frac{\partial T}{\partial x} = 0 \quad \text{at} \quad x \rightarrow -\infty \quad (3.10)$$

and

$$a^2 T^n \frac{\partial T}{\partial r} \Big|_{a^+} = \lambda L + a^2 (AP_m)^{1/2} \frac{\partial T}{\partial x} \Big|_{0^-} \quad \text{at} \quad r = a \quad (3.11)$$

3.2 Gas Phase

The dimensionless conservation equations to describe the gas phase are:

$$p_m \frac{\partial \rho}{\partial \tau} + \frac{1}{r^2} \frac{\partial}{\partial r} (r^2 \rho u) = 0 \quad (3.12)$$

$$p_m \frac{\partial(\rho T)}{\partial \tau} + \frac{1}{r^2} \frac{\partial}{\partial r} (r^2 \rho u T) - \frac{1}{r^2} \frac{\partial}{\partial r} \left(r^2 T^n \frac{\partial T}{\partial r} \right) = 0 \quad (3.13)$$

$$p_m \frac{\partial(\rho Y_F)}{\partial \tau} + \frac{1}{r^2} \frac{\partial}{\partial r} (r^2 \rho u Y_F) - \frac{1}{r^2} \frac{\partial}{\partial r} \left(\frac{r^2 T^n}{Le_F} \frac{\partial Y_F}{\partial r} \right) = 0 \quad (3.14)$$

$p_m \equiv \varepsilon P_m$ in which $\varepsilon \equiv \rho_\infty^* / \rho_l^*$ is the ratio of gas phase density to liquid phase density. In previous works (CRISTALDO; FACHINI, 2013a; CRISTALDO; FACHINI, 2013b), the multiplication εP_m was considered much smaller than one $p_m \ll 1$ and the transient terms of the equations were neglected. In the current work $p_m \sim O(1)$ and the value of the density ratio ε is varied in order to simulate different ambient pressure conditions. Le_F is the vapor Lewis number.

The boundary condition at the droplet surface is:

$$\left. \frac{r^2 T^n}{Le_F} \frac{\partial Y_F}{\partial r} \right|_{a^+} = \lambda (Y_{Fs} - 1) \quad \text{at} \quad r = a \quad (3.15)$$

The subscript s stands for the condition at the droplet surface. The fuel mass fraction at the droplet surface is related to the temperature at the same place by the Clausius – Clapeyron relation.

$$Y_{Fs} = \exp \left[\gamma \left(1 - \frac{1}{T_s} \right) \right] \quad (3.16)$$

where $\gamma \equiv L^* M_F^* / (R_0^* T_b^*)$ is a function of the latent heat of vaporization L^* , the fuel molecular weight M_F^* , the universal gas constant R_0^* and the boiling temperature T_b^* .

Far from the droplet the following conditions are assumed:

$$T = T_\infty \quad \text{and} \quad Y_F = 0 \quad \text{for} \quad r \rightarrow +\infty \quad (3.17)$$

3.2.1 Stream function

Using the material function $\psi = p_m \int r^2 \rho dr$ as spatial coordinate the problem can be simplified. That function satisfies $\psi_r = p_m r^2 \rho$ and $\psi_\tau = -r^2 \rho u$, ($p_m \equiv \varepsilon P_m$).

Thereby, Eqs. (3.12),(3.13) and (3.14) can be re-written as

$$\psi_{r\tau} - \psi_{\tau r} = 0 \quad (3.18)$$

$$\frac{\partial T}{\partial \tau} - \frac{\partial}{\partial \psi} \left(\tilde{D} \frac{\partial T}{\partial \psi} \right) = 0 \quad (3.19)$$

$$\frac{\partial Y_F}{\partial \tau} - \frac{\partial}{\partial \psi} \left(\frac{\tilde{D}}{Le_F} \frac{\partial Y_F}{\partial \psi} \right) = 0 \quad (3.20)$$

which $\tilde{D} = p_m r^4 \rho T^n$. The boundary conditions in the new variable are

$$\tilde{D} \frac{\partial T}{\partial \psi} \Big|_{r=a} = a^2 (AP_m)^{1/2} \frac{\partial T}{\partial x} \Big|_{x=0^-} + \lambda L \quad \text{at } r = a \quad (3.21)$$

$$- \frac{\tilde{D}}{Le_F} \frac{\partial Y_F}{\partial \psi} \Big|_{r=a} = \lambda (Y_{Fs} - 1) \quad \text{at } r = a \quad (3.22)$$

in which $Le_F = \alpha_\infty^* / D_{F\infty}^*$

4 NUMERICAL CODE

4.1 Numerical strategy

The problem is solved considering a n-heptane ferrofluid droplet in a quiescent inert atmosphere with temperature T_∞ and vapor mass fraction $Y_{F\infty} = 0$. The problem is numerically solved by following the procedure:

- a) An initial guess for the vaporization rate λ and the surface temperature T_s are provided, knowing the droplet radius, which initially is $a = 1$
- b) Temperature and mass fraction profiles are determined by integrating Eqs (3.9), (3.13) and (3.14). The differential equations are solved by an explicit finite difference scheme.
- c) Once the temperature and mass fraction profiles in both sides of the droplet surface are known, the boundary conditions, Eqs. (3.11) and (3.15), are calculated. If they are not satisfied, new vaporization rate λ and new droplet surface temperature T_s are chosen via Newton-Raphson method. The process is repeated until the boundary conditions Eqs. (3.11) and (3.15) to be satisfied.
- d) The steps b and c are repeated. Since $P_m \gg 1$, the radius variation is very small for $\tau = O(1)$. The effect of the magnetic nanoparticle fraction variation can be neglected during the heating process because of very small volume variation for the droplet.
- e) The process is repeated until any point inside the droplet to reach boiling temperature.

4.2 Discretization

In order to find the numerical solution of the set of equations, first it is necessary to transform them into a discrete form. By doing that, the equations become suitable for numerical evaluation and implementation on digital computers.

In this chapter the discretization of the governing equations and their boundary conditions are shown.

4.2.1 Liquid Phase

From the mass conservation equation, it is possible, through use of derivative approximation (FERZIGER; PERIC, 2002), to calculate the radius variation of the droplet. Knowing that

$$\left. \frac{d\phi}{d\omega} \right|^i = \frac{\phi^{i+1} - \phi^i}{\Delta\omega} \quad (4.1)$$

then Eq. (3.7) becomes

$$\frac{(a^{i+1})^3 - (a^i)^3}{\Delta\tau} = -3 \frac{\lambda^i}{P_m} \quad (4.2)$$

For the energy conservation equation considering a constant mesh spacing

$$\left. \frac{\partial^2 T}{\partial x^2} \right|_j^i = \frac{T_{j+1}^i + T_{j-1}^i - 2T_j^i}{(\Delta x)^2} \quad (4.3)$$

then Eq. (3.9) becomes

$$\frac{T_j^{i+1} - T_j^i}{\Delta\tau} = \frac{T_{j+1}^i + T_{j-1}^i - 2T_j^i}{(\Delta x)^2} + \frac{f^2 T_j^i}{(T_j^i)^2 + f^2}$$

or

$$T_j^{i+1} = T_j^i + \frac{\Delta\tau}{(\Delta x)^2} [T_{j+1}^i + T_{j-1}^i - 2T_j^i] + \Delta\tau \frac{f^2 T_j^i}{(T_j^i)^2 + f^2} \quad (4.4)$$

Using the same procedure in the boundary condition, Eq. (3.11), becomes

$$\tilde{D}_s^i \left(\frac{T_2^i - T_s^i}{\psi_2^i - \psi_s^i} \right) \Big|_{gas} = \lambda^i L + (a^i)^2 (P_m A)^{\frac{1}{2}} \left(\frac{T_s^i - T_2^i}{\Delta x} \right) \Big|_{liquid} \quad (4.5)$$

in which $\tilde{D}_k^i \equiv (r_k^i)^2 (T^{1/2})_k^i (\psi_r)_k^i = p_m (r_k^i)^4 (T^{1/2})_k^i \rho_k^i$. The subscript i is the temporal reference, j is the spatial reference relative to the liquid domain and k is the spatial reference relative to the the gas domain.

The coordinate radius - ψ conversion is calculated by relation $\psi_r = p_m r^2 \rho$ which in the discrete form becomes:

$$\frac{\psi_{k+1}^i - \psi_k^i}{r_{k+1}^i - r_k^i} = p_m(r_k^i)^2 \rho_k^i \quad (4.6)$$

4.2.2 Gas Phase

Following the same procedure used before, with the derivative approximation for non-constant mesh spacing (FERZIGER; PERIC, 2002)

$$\frac{\partial}{\partial \psi} \left[\tilde{D} \frac{\partial T}{\partial \psi} \right] \Big|_k^i = \frac{2}{\psi_{k+1}^i - \psi_{k-1}^i} \left[\left(\tilde{D} \frac{\partial T}{\partial \psi} \right) \Big|_{k+1/2}^i - \left(\tilde{D} \frac{\partial T}{\partial \psi} \right) \Big|_{k-1/2}^i \right] \quad (4.7)$$

with

$$\tilde{D} \frac{\partial T}{\partial \psi} \Big|_{k+1/2}^i = \tilde{D} \Big|_{k+1/2}^i \left(\frac{T_{k+1}^i - T_k^i}{\psi_{k+1}^i - \psi_k^i} \right) \quad (4.8)$$

$$\tilde{D} \frac{\partial T}{\partial \psi} \Big|_{k-1/2}^i = \tilde{D} \Big|_{k-1/2}^i \left(\frac{T_k^i - T_{k-1}^i}{\psi_k^i - \psi_{k-1}^i} \right) \quad (4.9)$$

then substituting Eqs. (4.8) and (4.9) into Eq. (4.7) the energy conservation equation, Eq. (3.19), becomes

$$\frac{T_k^{i+1} - T_k^i}{\Delta \tau} = \frac{2}{\psi_{k+1}^i - \psi_{k-1}^i} \left[\tilde{D} \Big|_{k+1/2}^i \left(\frac{T_{k+1}^i - T_k^i}{\psi_{k+1}^i - \psi_k^i} \right) - \tilde{D} \Big|_{k-1/2}^i \left(\frac{T_k^i - T_{k-1}^i}{\psi_k^i - \psi_{k-1}^i} \right) \right]$$

or

$$T_k^{i+1} = T_k^i + \left\{ \frac{2}{\psi_{k+1}^i - \psi_{k-1}^i} \left[\tilde{D} \Big|_{k+1/2}^i \left(\frac{T_{k+1}^i - T_k^i}{\psi_{k+1}^i - \psi_k^i} \right) + \right. \right. \\ \left. \left. - \tilde{D} \Big|_{k-1/2}^i \left(\frac{T_k^i - T_{k-1}^i}{\psi_k^i - \psi_{k-1}^i} \right) \right] \right\} \Delta \tau \quad (4.10)$$

recalling that $\tilde{D}_k^i \equiv (r_k^i)^2 (T^{1/2})_k^i (\psi_r)_k^i = p_m(r_k^i)^4 (T^{1/2})_k^i \rho_k^i$, then $\tilde{D}_{k+1/2}^i \equiv (p_m(r_{k+1}^i)^4 (T^{1/2})_{k+1}^i \rho_{k+1}^i - p_m(r_k^i)^4 (T^{1/2})_k^i \rho_k^i) / 2$ and $\tilde{D}_{k-1/2}^i \equiv (p_m(r_k^i)^4 (T^{1/2})_k^i \rho_k^i - p_m(r_{k-1}^i)^4 (T^{1/2})_{k-1}^i \rho_{k-1}^i) / 2$.

In the same way, the species conservation Eq. (3.20) is found

$$Y_{F_k}^{i+1} = Y_{F_k}^i + \left\{ \frac{2}{Le_F(\psi_{k+1}^i - \psi_{k-1}^i)} \left[\tilde{D} \Big|_{k+1/2}^i \left(\frac{Y_{F_{k+1}}^i - Y_{F_k}^i}{\psi_{k+1}^i - \psi_k^i} \right) + \right. \right. \\ \left. \left. - \tilde{D} \Big|_{k-1/2}^i \left(\frac{Y_{F_k}^i - Y_{F_{k-1}}^i}{\psi_k^i - \psi_{k-1}^i} \right) \right] \right\} \Delta\tau \quad (4.11)$$

The boundary condition Eq. (3.22) for species conservation at the droplet surface leads to

$$\tilde{D}_s^i \left(\frac{Y_{F_2}^i - Y_{F_s}^i}{\psi_2^i - \psi_s^i} \right) \Big|_{gas} = Le_F \lambda^i \left(Y_{F_s}^i - 1 \right) \quad (4.12)$$

5 RESULTS

The base fluid of the ferrofluid droplet in this work is n-heptane. The droplet has radius of $r_0^* = 500\mu\text{m}$. The magnetic nanoparticle is of magnetite ($\gamma\text{Fe}_2\text{O}_3$) of radius $r_n^* = 6\text{ nm}$, density $\rho_n^* = 5180\text{ kg}/\text{m}^3$, specific heat $c_n^* = 670\text{ J}/(\text{kg K})$ and thermal conductivity $k_n^* = 23\text{ J}/(\text{m s K})$. The thickness of the nanoparticle coating layer is of $\delta_N = 1\text{ nm}$, domain magnetization is $M_d^* = 414\text{ kA}/\text{m}$, and volume fraction of nanoparticles $\Phi = 0.07$. The intensity of the magnetic field is $B_0 = \mu_0 H_0^* = 0.28\text{ Tesla}$. Uniform temperature and nanoparticle concentration profile in the liquid phase and temperature and fuel concentration in the gas phases are assumed as initial condition. In the liquid phase the initial temperature T_0^* was set equal to 297.24 K , which corresponds to $T_0 \equiv T_0^*/T_b^* = 0.8$ (the boiling temperature $T_b^* = 371.55$ for ambient pressure). In the gas phase, temperature T_∞^* take values from 334.39 K to 2229.3 K ($0.9 \leq T_\infty \leq 6$). The results presented in this section correspond to two models.

The first set of results from the first model describes strictly the influence of the transient processes of energy and mass accumulation in the gas phase. For that, the effect of nanoparticle concentration on the thermal conductivity of the ferrofluid is neglected. Also, the value of the parameter p_m is changed only with the variation of the ambient pressure. However, the properties, which depend on the pressure, are kept artificially unchanged, i.e., boiling temperature, latent heat and transport coefficients. This model is defined as constant properties model.

The second set of results, from the second model, shows the effect of an effective liquid phase thermal conductivity, boiling temperature, latent heat and transport coefficients on the droplet heating and vaporization. That model is defined as variable properties model.

Both models stop when, at any point inside the droplet, boiling temperature is reached. The model is not valid at any moment further ($T > 1$ for $r < a$ and $x < 0$) due to bubble formation inside the droplet. Lewis number is set equal unit.

5.1 Constant property model

Transient effects of the gas phase on the droplet heating and vaporization are analyzed through the change of value of the density ratio ε , without concerning the variation of other properties with pressure. The ambient temperature T_∞^* is set

equal to 334.39 K ($T_\infty = 0.9$), 1114.65 K ($T_\infty = 3.0$) and 2229.3 K ($T_\infty = 6.0$) with the reference temperature equal to that of the boiling condition ($T_b^* = 371.66\text{ K}$) for atmospheric pressure. For this condition, the latent heat of vaporization is $L^* = 316.76\text{ kJ/kg}$. For p_m , values of 0.01, 0.1, 1.0, 2.0 and 5.0 are assigned. Frequency of the magnetic field is varied from $f = 0.3$ to values in which relaxation processes of the nanoparticle reaches saturation (approximately $f \sim 5.0$). For frequencies lower than 0.3 the thickness of the thermal boundary layer, $\delta = [A/(P_m f^2)]^{1/2}$, becomes of the same order of the droplet radius and the model is no longer valid. Recalling, the simulation is performed until any point of the droplet reaches boiling temperature.

The time in which the boiling condition is achieved is defined as heating time t_h^* . After that, bubble formation takes place causing the droplet break up. In case of no droplet break up, the model is still not valid due to the presence of two phases inside the droplet.

The validation of the code is not presented in the following as usual in text of numerical simulation. The code validation will be done comparing the evolution of the vaporization rates obtained by the code imposing the condition $p_m \ll 1$ and by the quasi-steady approximation $p_m = 0$. The validation discussion is postponed to the end of the section because some physical processes must be introduced and discussed, which will justify the code validation.

The condition addressed in this problem leads to a magnetic power much larger than the thermal power ($P_m \gg 1$), $P_m = 100$ specifically. Under that assumption, uniform temperature profile is found inside the droplet, except in a thin region close to its surface which is defined as thermal boundary layer (FACHINI; BAKUZIS, 2010; CRISTALDO; FACHINI, 2013a; CRISTALDO; FACHINI, 2013b). In the current model, the droplet heating and vaporization occur due to the heat flux provided by the environment and the magneto relaxation source. Results point out that the former process is dependent on the difference of the ambient and droplet surface temperature, meanwhile the latter process depends on the temperature profile inside the droplet, according to the right hand side of Eq. (3.9). Because of such dependencies, the time evolution of the droplet temperature changes with the initial conditions.

For the cases of ambient temperature below the boiling temperature (defined as cooling case), the heating process can be divided into two periods. The first one is determined meanwhile the ambient temperature is larger than the droplet surface temperature. The droplet heating takes place due to the magneto relaxation source

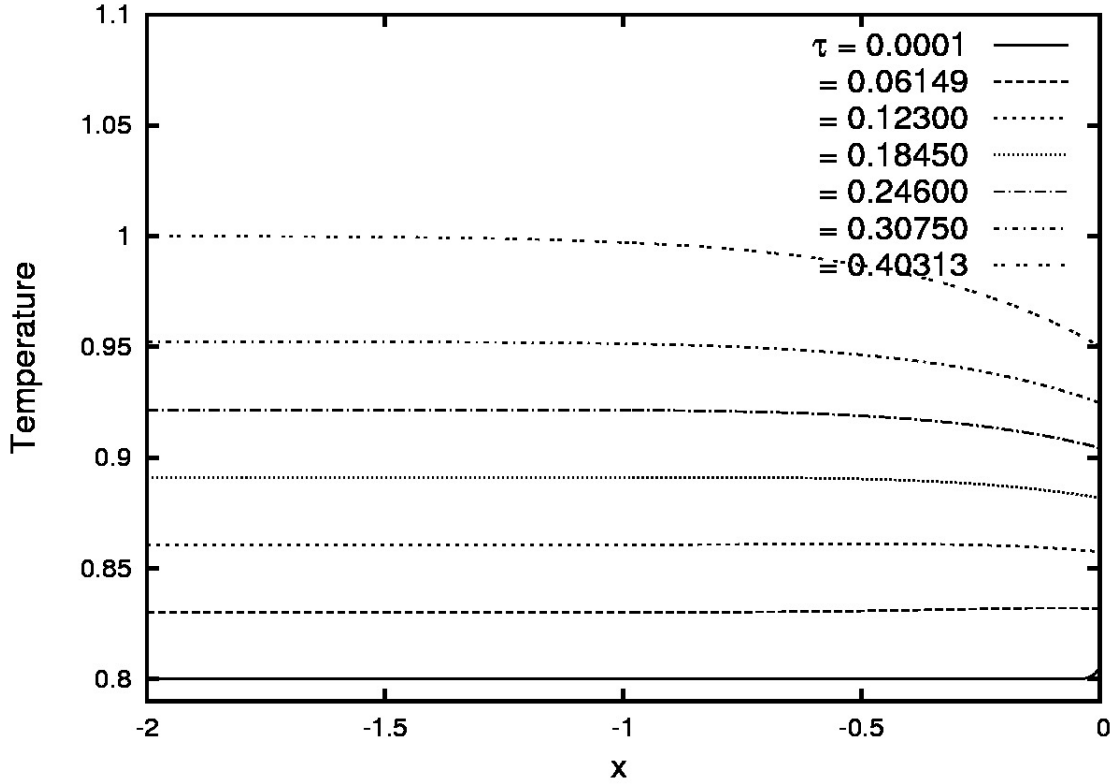


Figure 5.1 - Temperature profile inside the droplet $p_m = 1.0$ and $f = 1.0$ for $T_\infty = 0.9$ ($T_\infty^* = 334.39$ K).

inside the droplet and the heat flux from the gas phase. In this period, the temperature profile in the thermal boundary layer is slightly higher than that of the droplet core, Fig. 5.1, for $\tau = 0.06149$.

After that, the heating process starts the second period. Now, the magneto relaxation source is the main process in the droplet heating process. In this heating period the droplet surface temperature may or may not be higher than the ambient temperature. Under this condition, the temperature of the droplet core increases faster than that of the thermal boundary layer. The consequence is a negative temperature gradient in the thermal boundary layer, indicating that the magneto relaxation heating is the process controlling the heating and vaporization. Therefore, for the cooling cases the boiling condition is found in the droplet core.

For the cases of ambient temperature above the boiling condition, the heating process has a single behavior, differently from the cooling case. The heat transfer from the gas phase is always compared with magneto relaxation source and it imposes a temperature profile in the thermal boundary layer always higher than that of the

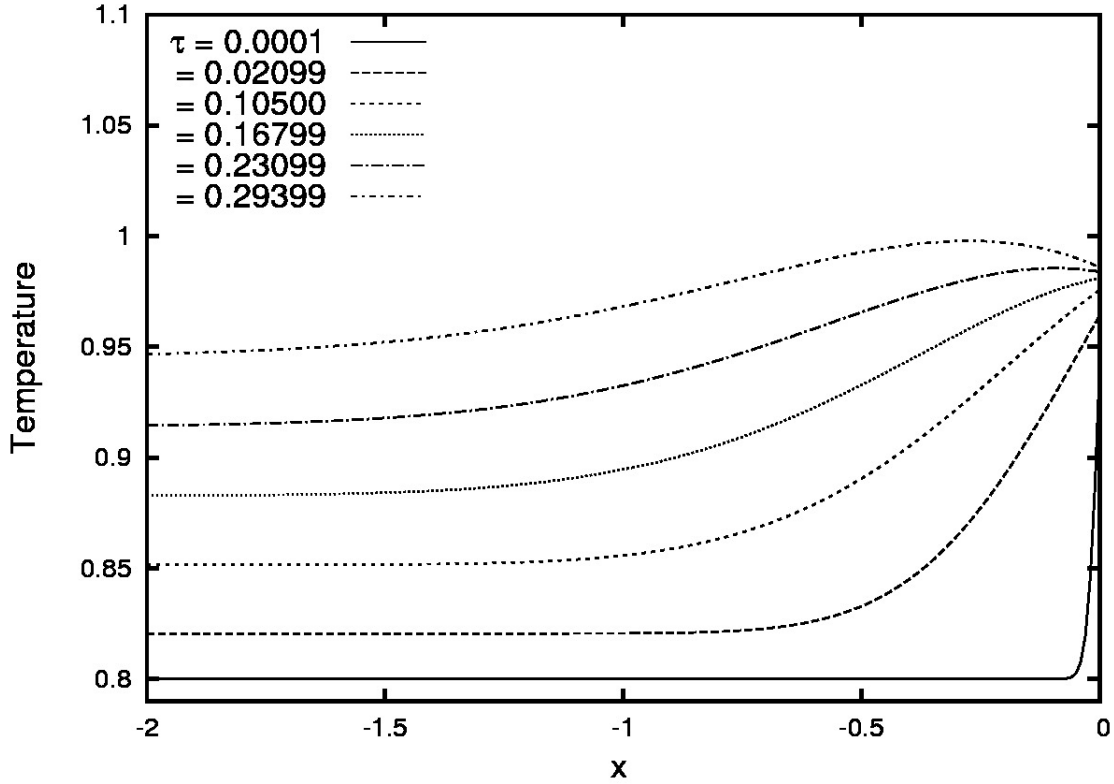


Figure 5.2 - Temperature profile inside the droplet $p_m = 1.0$ and $f = 1.0$ for $T_\infty = 3.0$ ($T_\infty^* = 1114.65$ K).

droplet core. Since magneto relaxation source depends on temperature, the temperature inside the thermal boundary layer will increase more than that of the core. The droplet surface temperature follows the evolution of the thermal boundary layer up to the moment that the heat loss by vaporization becomes significant on the determination of that temperature, as can be seen in Fig. 5.2 for $\tau = 0.168$.

After that, the temperature inside the thermal boundary layer increases faster than that of the droplet surface. A local maximum of temperature appears in the thermal boundary layer, as observed in previous analysis (FACHINI; BAKUZIS, 2010; CRISTALDO; FACHINI, 2013a; CRISTALDO; FACHINI, 2013b). The maximum on temperature profile imposes a negative temperature gradient from the thermal boundary layer to the droplet surface and it is responsible for larger vaporization rates, as shown in Fig. 5.3.

As seen on the results of Fig 5.1 the magneto relaxation source ensures that the boiling condition is always achieved, with large or small positive temperature gradients in the gas phase, or even with negative ones.

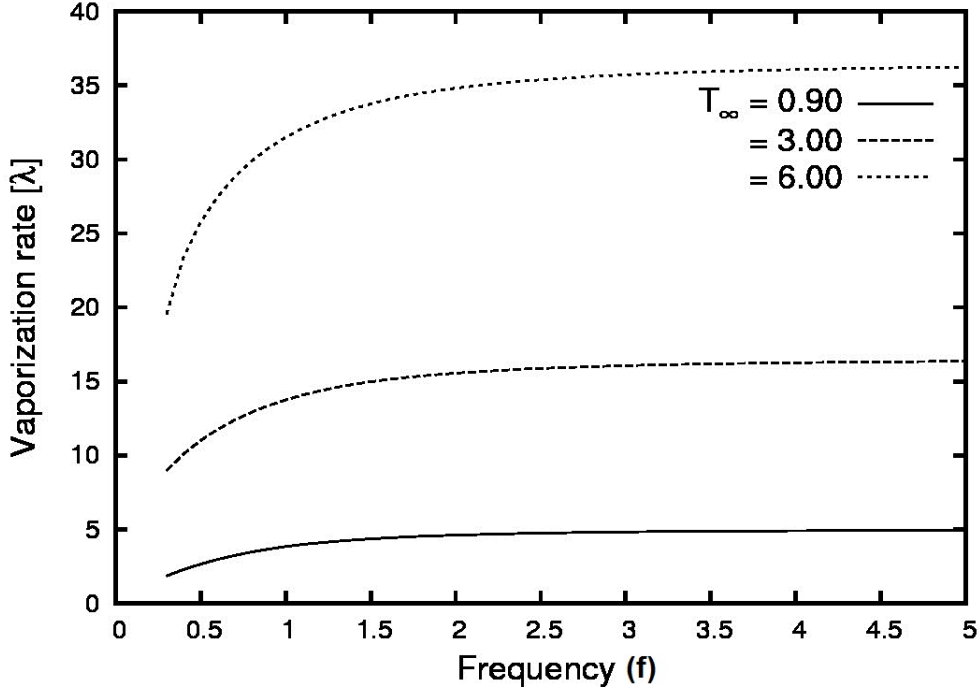


Figure 5.3 - Vaporization rate as a function of frequency for different ambient temperatures $T_{\infty} = 0.9$ ($T_{\infty}^* = 334.39$ K), $T_{\infty} = 3.0$ ($T_{\infty}^* = 1114.65$ K), $T_{\infty} = 6.0$ ($T_{\infty}^* = 2229.3$ K), for $p_m = 1.0$.

In Figure 5.3 the influence of the ambient temperature T_{∞} and the frequency f on the vaporization rate λ are exhibited. Reduction on the heat flux from the gas phase to the droplet (decrease of T_{∞}) makes the effect of magneto relaxation source to dominate the heating and vaporization processes. This characteristic is confirmed analyzing the absolute effect on Fig. 5.3. For $T_{\infty} = 6$, an increase of the frequency from 0.3 to 5 results in an increase of about 85% on the vaporization rate. Meanwhile, for $T_{\infty} = 0.9$, an increase of the frequency from 0.3 to 5 results in an increase of about 168% on the vaporization rate.

In general, the vaporization rate is controlled by the ambient atmospheric temperature (T_{∞}), as seen in Fig. 5.3.

The influence of the field frequency and the ambient temperature on the droplet surface temperature becomes more clear from Fig. 5.4. Like the vaporization rate, the droplet surface temperature T_s is mainly controlled by the ambient temperature T_{∞} (or external heat flux), as already shown in the classical theory. The magnetic relaxation heating through the frequency has only a slight effect on the vaporization for the low ambient temperature $T_{\infty} = 0.9$ in the range of $0.3 < f < 1$. The strong

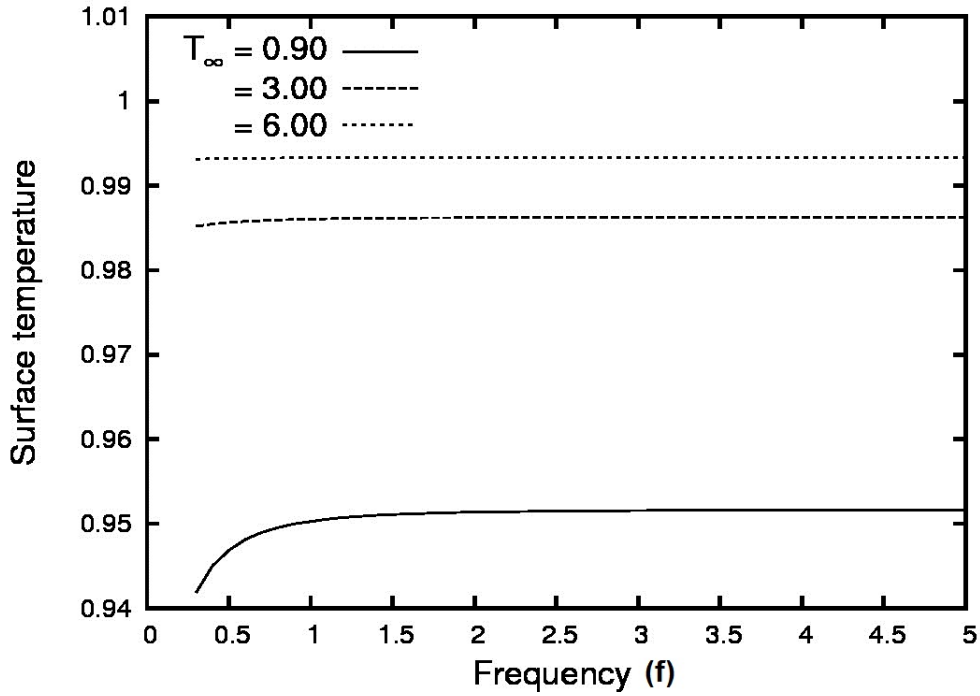


Figure 5.4 - Surface temperature as a function of frequency for different ambient temperatures $T_\infty = 0.9$ ($T_\infty^* = 334.39$ K), $T_\infty = 3.0$ ($T_\infty^* = 1114.65$ K), $T_\infty = 6.0$ ($T_\infty^* = 2229.3$ K), for $p_m = 1.0$.

influence of the magneto relaxation heating is on droplet heating time, as will be shown ahead.

In Figure 5.5 the droplet heating time for different ambient temperatures as a function of the field frequency is shown. As expected at low field frequencies f , the heating process is dependent on both the heat flux from the gas phase and the magneto relaxation source. While for high field frequencies the heating and vaporization processes are practically dominated by the magnetic process. By setting the field frequency equal to $f = 0.3$ and comparing the ambient temperatures $T_\infty = 0.9$ and $T_\infty = 6.0$, it is seen that the change on the ambient temperature results in a heating time reduction (denominated as τ_{hr}) of about $\tau_{hr} \sim 0.75$. By setting the field frequency equal to $f = 5.0$, by comparing the same ambient temperatures the heating time reduction is of about $\tau_{hr} \sim 0.1$. It can be better explained by analyzing the magneto relaxation source, right hand side of Eq. (3.9) $f^2 T / (T^2 + f^2)$. At low field frequencies, the magneto relaxation source can be approximated to $\sim f^2 / T$. It is seen that an increase on the temperature causes a reduction on the magneto relaxation source. Under this condition, the gas-phase heat flux is the process controlling the heat and droplet vaporization. On the other hand, at high field frequencies the

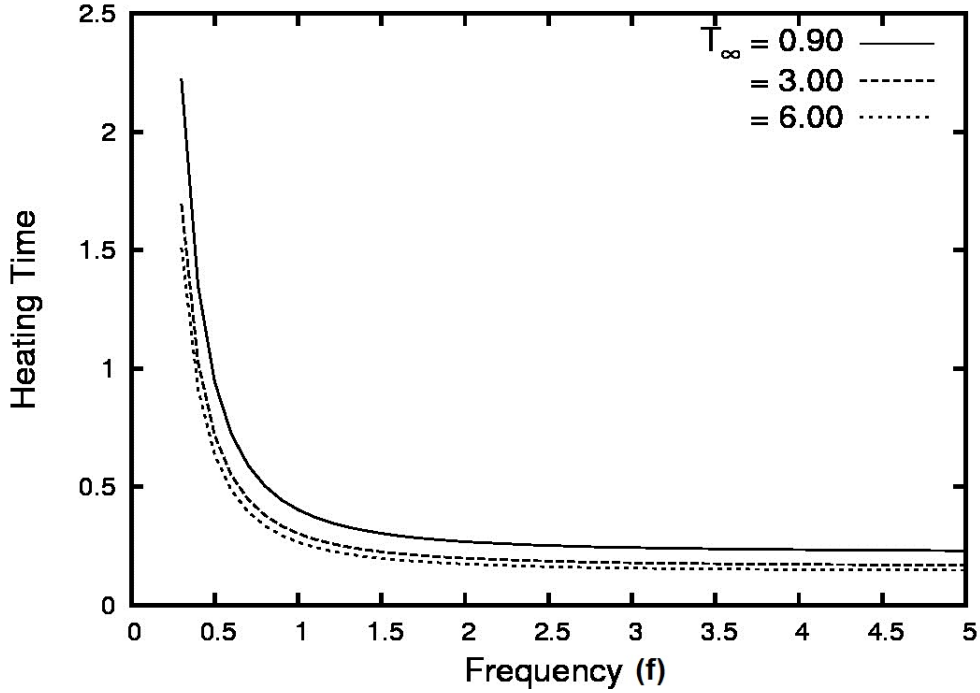


Figure 5.5 - Heating time as a function of frequency for different ambient temperatures $T_{\infty} = 0.9$ ($T_{\infty}^* = 334.39$ K), $T_{\infty} = 3.0$ ($T_{\infty}^* = 1114.65$ K), $T_{\infty} = 6.0$ ($T_{\infty}^* = 2229.3$ K), for $p_m = 1.0$.

magnetic term can be approximated to $\sim T$. Under such assumptions, the magnetic relaxation is accelerated with temperature, and it is the main process on droplet heating, as seen on Fig. 5.5.

Until now, magnetic field frequency was fixed and two temperatures were chosen to be compared. That was useful to demonstrate when the magneto relaxation source is the controlling process of the problem. In order to demonstrate the droplet heating time reduction generated by the magneto relaxation heating, a ambient temperature will be fixed and two values of field frequency will be chosen ($f = 0.3$ and $f = 5.0$). By doing that, results have shown a heating time reduction of about 7.5 times.

Results demonstrated that for frequencies higher than one ($f > 1$) saturation of the magnetic process can be observed. Such behavior is also described in a previous work (CRISTALDO; FACHINI, 2013a) in which a quasi-steady case is studied. The saturation is a consequence of the magnetic nanoparticles to be unable to change its rotation at the same speed of the magnetic field intensity changes. The characteristic time of the nanoparticle to adapt a new conditions is much larger than the magnetic field period.

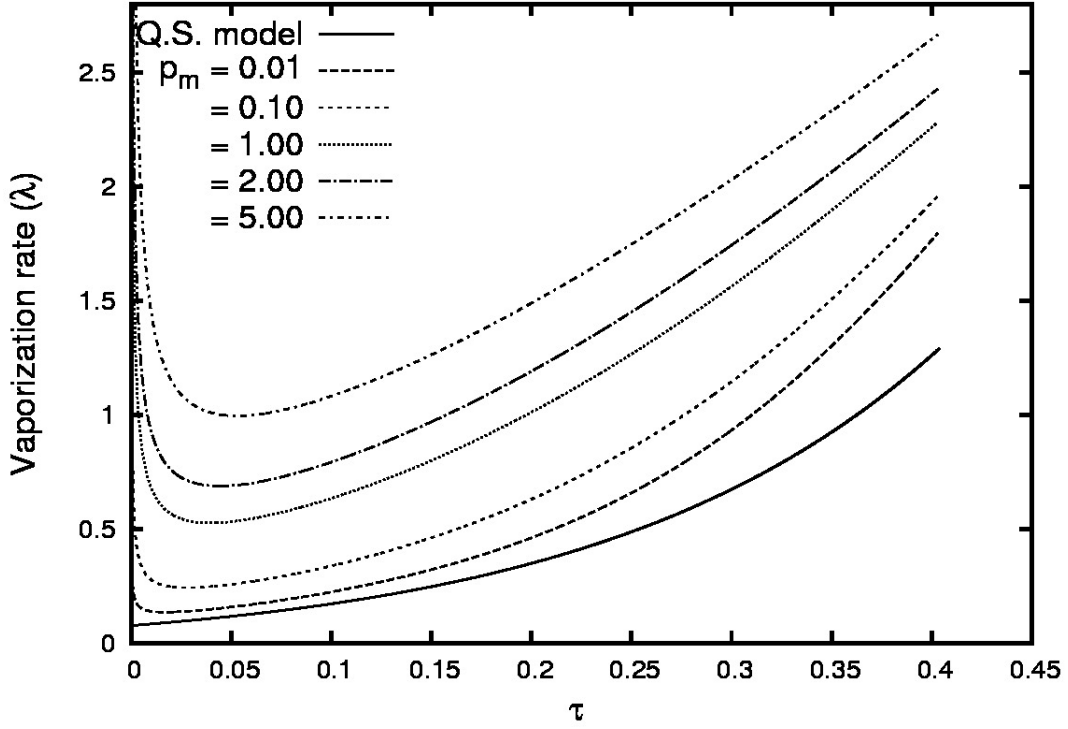


Figure 5.6 - Vaporization rate as a function of time for different p_m regimes, $T_\infty = 0.9$ ($T_\infty^* = 334.39$ K) and $f = 1.0$.

The validation of the code is performed by comparing the results of the transient model for the condition $p_m = 0.01$ with that of the quasi-steady model ($p_m = 0$) (CRISTALDO; FACHINI, 2013a), Fig. 5.6.

The current model showed good agreement with the quasi-steady model. Even with a large difference between the vaporization rates for $p_m = 0$ and $p_m = 0.01$ at the end of the heating time, it is possible to say that the current model is validated. The justification for that difference is based on the fact that the magneto relaxation source is strongly dependent on the initial condition. The quasi-steady results consider a completely developed profile for each time step, while the transient model has to evolve to that condition. Because of that, a difference in the temperature gradients at the droplet surface will be present, causing a different time evolution on the temperature profile. That makes the temperature profile inside the thermal boundary layer to rise more quickly in the transient model than in the quasi-steady model which causes the difference between the models.

It is also seen on Figure 5.6 that the vaporization rate does not scale in the same way with the pressure in the range $0.01 \leq p_m \leq 1$ and $1 \leq p_m \leq 5$. The

transient accumulation enhances the temperature gradients at the droplet surface, which modifies the heat flux towards the droplet. Recalling that the magneto relaxation source is dependent on initial condition, the change of heat flux alters the temperature evolution inside the droplet. As the heat flux variation is large in the range $0.01 \leq p_m \leq 1$ and slight in $1 \leq p_m \leq 5$, it will result in higher variation in the vaporization rates in the former range than in the latter. Again, the data exhibited on Fig. 5.6 confirm that the heating time is controlled practically by the magneto relaxation heating: changing p_m by maintaining fixed the value of the frequency, the heating time is practically the same for all cases for higher frequencies.

5.2 Variable property model

The previous results are determined imposing changes on ε via ambient pressure but keeping the thermodynamic properties unchanged with values corresponding to normal ambient pressure. Unlike previous model, in this model the thermodynamic properties will have proper values following the ambient pressure. Then, the boiling temperature of n-heptane is approximated by the expression

$$T_b^* = 59.026 \ln(P^*) + 477.114 \quad (5.1)$$

in which the pressure P^* is in MPa .

Through use of the Clapeyron equation

$$\frac{d \log P^*}{d(1/T^*)} = - \frac{L^*}{2.303 R^* (Z_g - Z_l)} \quad (5.2)$$

and the Haggemacher correlation ([HAGGENMACHER, 1946](#))

$$Z_g - Z_l = \left(1 - \frac{P_r^*}{T_r^{*3}}\right)^{1/2} \quad (5.3)$$

an expression for the latent heat of vaporization is obtained.

$$L^* = 2.303 R^* \left(\frac{T_1^* T_2^*}{T_1^* - T_2^*} \log \frac{P_2^*}{P_1^*} \right) \left(1 - \frac{P_r}{T_r^3}\right)^{1/2} \quad (5.4)$$

Substituting the critical and saturation properties into Eq. 5.4, the Klein equation, as seen in (FISHTINE, 1963), is described in its usual form.

$$L^* = 4.576 \frac{T^* \log(P_r) \sqrt{1 - P_r/T_r^3}}{T_r - 1} \quad (5.5)$$

The variables Z_g , Z_l , $P_r \equiv P^*/P_{crit}^*$ and $T_r \equiv T^*/T_{crit}^*$ are the compressibility factor for the vapor and the liquid and the reduced pressure and temperature, respectively. The units of L^* are calories per mole if the temperature T^* is in K and B.t.u. per mole if the temperature is in $^{\circ}R$ (FISHTINE, 1963).

In the liquid phase, the presence of nanoparticles leads to effective properties (MAENOSONO; SAITA, 2006),

$$c_{l\ ef}^* = (1 - \phi)c_l^* + \phi c_n^*, \quad \rho_{l\ ef}^* = (1 - \phi)\rho_l^* + \phi \rho_n^* \quad (5.6)$$

in which ϕ is the volume fraction of nanoparticles. The subscript l stands for the properties of the fluid and n for the nanoparticle properties. As cited before, the nanoparticles are surface-coated (nanolayer), which is accounted in the calculation of the nanoparticle effective thermal conductivity.

The thermal conductivity of the nanolayer is an intermediate value between that of solid and liquid. From the modified Maxwell equation (YU et al., 2000; YU; CHOI, 2003)

$$k_{l\ ef}^* = k_l^* \left[\frac{k_n^* + 2k_n^* + 2\phi(k_n^* - k_l^*)(1 + \beta)^3}{k_n^* + 2k_n^* - \phi(k_n^* - k_l^*)(1 + \beta)^3} \right] \quad (5.7)$$

in which β is the ratio of the nanolayer thickness to the nanoparticle radius.

Recalling, this model considers a single n-heptane droplet of radius of $500\mu m$ containing a volume fraction $\phi = 0.07$ of stable and homogeneously dispersed nanoparticles of magnetite of radius $6nm$. Physical properties of the nanoparticles are: domain magnetization ($M_d^* = 414$ kA/M), thermal conductivity ($k_n^* = 23$ J/m s K), specific heat ($c_{pl}^* = 670$ J/kg K), and density ($\rho_n^* = 5180$ kg/m³). The droplet is placed in an ambient atmosphere at temperature of $T_{\infty}^* = 1000K$ with different pressures (from 0.36 atm to 25 atm). As in the first model, the droplet is exposed to an external alternating magnetic field with different frequencies. The assumption of very high

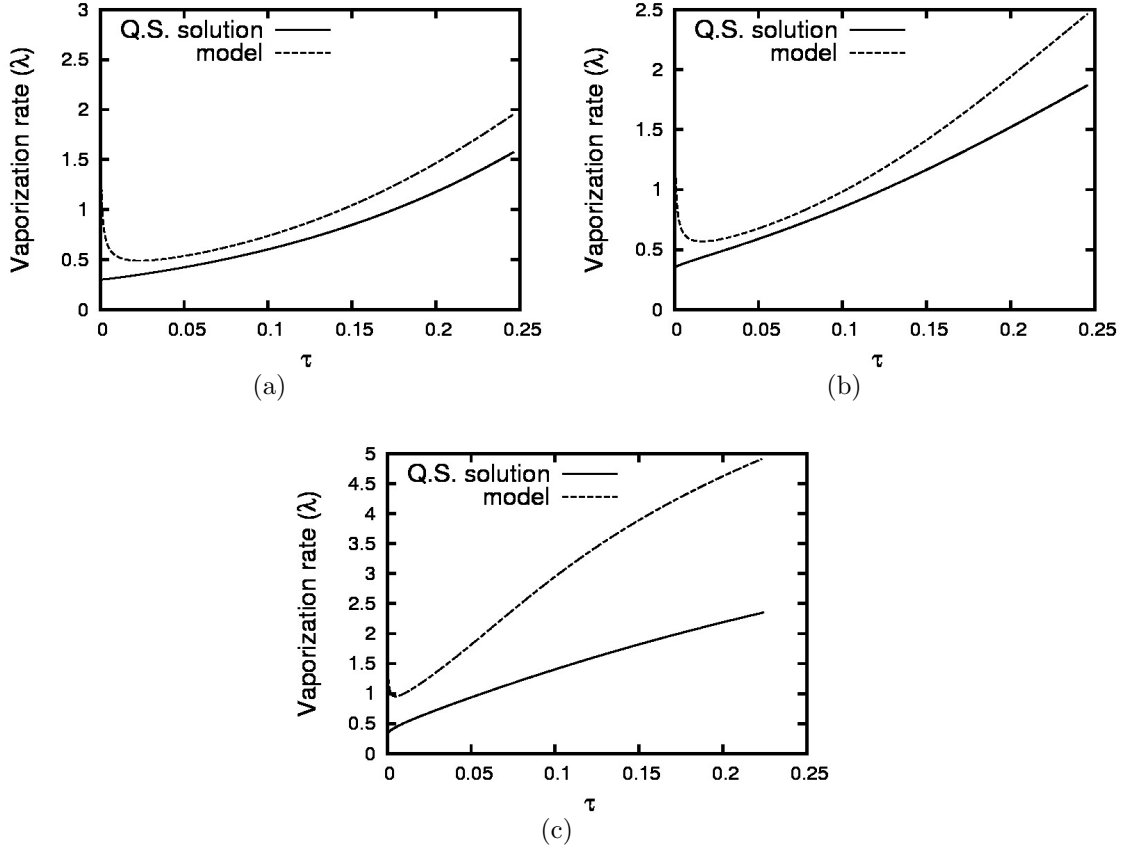


Figure 5.7 - Validation: vaporization rate as a function of time for pressure $P^* = 0.36$ atm and ambient temperature a) $T_\infty^* = 305$ K, b) 500 K, c) 1000 K corresponding to $p_m = 0.044, 0.027, 0.013$, respectively.

magnetic power ($P_m \gg 1$) is obtained by application of high intensity magnetic field, $H_0^* = 700 \text{ kA/m}$. The parameter P_m changes very little in the temperature range of the droplet problem, which justifies to take a constant value. Under addressed conditions, its value is $P_m = 100$.

The model validation is obtained by comparing the results from the current model with pressure of 0.36 atm and that obtained by the quasi-steady model (Q.S solution) ($p_m = 0$) (CRISTALDO; FACHINI, 2013b) for different ambient temperatures ($T_\infty^* = 305, 500, 1000$ K). These conditions correspond to values of $p_m = 0.0438, 0.0267$ and 0.0134 , respectively. The results are shown in Fig. 5.7.

The present model presents a close agreement with the quasi-steady solution in term of the heating time and vaporization rate for the case $T_\infty^* = 305$ K. However, for the other temperatures, the results are in agreement in terms of the heating time but not in terms of vaporization rate. The reason for that is, like in the constant

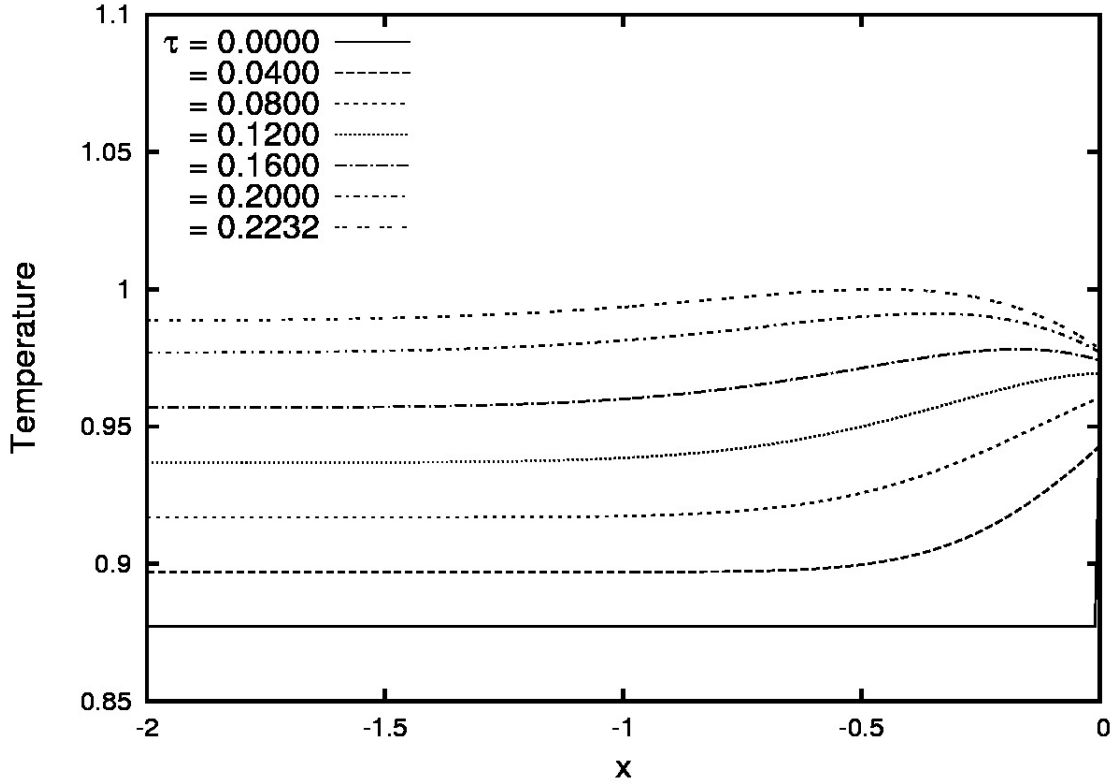


Figure 5.8 - Temperature evolution for condition of $p_m = 0.0134$ ($T_\infty^* = 1000$ K, $P^* = 0.36$ atm) and $f = 1$.

properties model, a larger heat flux from the gas phase to the droplet determined by the current model at the beginning of the heating process than that determined by the quasi-steady model. This difference on the heat flux changes the evolution and temperature profile inside the thermal boundary layer. Because of the strong dependence of the magneto relaxation heating on temperature, these differences in initial temperature evolution are increased during the heating process and the results are different vaporization regime. These results put in evidence that any non-uniformity on the initial temperature and/or nanoparticle distribution are responsible for different heating process. These results confirm the dependence of the heating and vaporization of a ferrofluid droplet on the initial conditions.

Figure 5.8 exhibits the temperature profiles at the heating time for the conditions $p_m = 0.0134$ ($P^* = 0.36$ atm and $T_\infty^* = 1000$ K) and $f = 1$. As in previous analysis (CRISTALDO; FACHINI, 2013a; CRISTALDO; FACHINI, 2013b), the boiling temperature occurs inside of the thermal boundary layer rather than at the surface, consequence of the magnetic relaxation heating, heat flux from the gas phase and heat loss due to vaporization at the droplet surface.

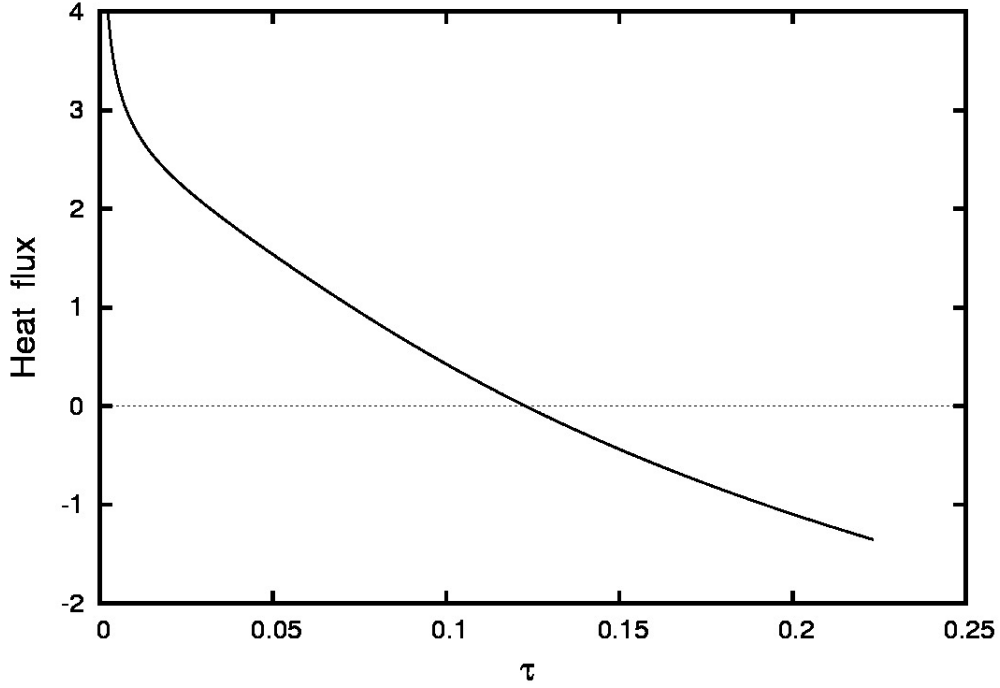


Figure 5.9 - Heat flux in the droplet surface (a^-) as a function of time for the condition of $p_m = 0.0134$ ($T_\infty^* = 1000$ K, $P^* = 0.36$ atm) and $f = 1$.

It is important to note that the numerical procedure is stopped when boiling condition is found at any position inside of the droplet because the model does not describe subsequent events, e.g., droplet explosion. The moment at which the boiling condition is found is defined by heating time, τ_h . There is a moment during the droplet heating that the temperature profile presents a local maximum inside the thermal boundary layer which is defined by maximum time, τ_{max} . The maximum on the temperature profile persists up to the heating time. Between the maximum time and heating time, the vaporization rate is increased by the addition of the heat flux from the thermal boundary layer to the droplet surface. Therefore, the increase of the thermal conductivity due to the magnetic nanoparticles (effective thermal conductivity) has a direct influence on the heat flux from the thermal boundary layer not only to the droplet core but also to the droplet surface. The consequences are thicker thermal boundary layer, high temperature core, high vaporization rate and longer heating time. All these processes are discussed in detail ahead.

Figure 5.9 exhibits the heat flux $(AP_m)^{1/2} \partial T / \partial x$ of Eq. 3.11 as a function of time. The main feature is the moment in which that flux crosses the zero value. It means that the thermal boundary layer starts transferring heat towards the droplet surface.

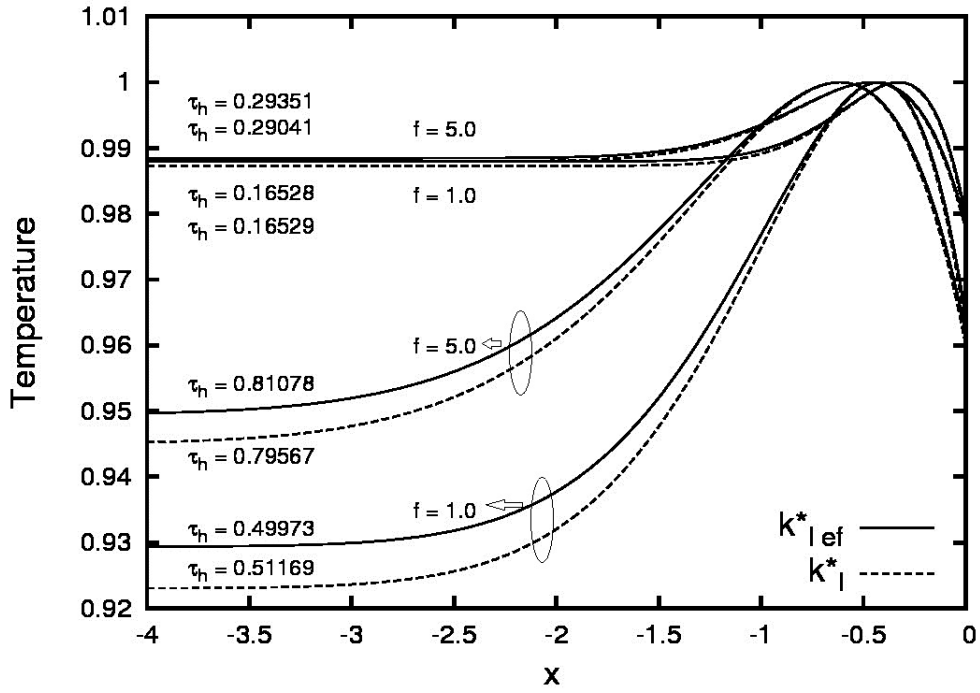


Figure 5.10 - Temperature profile at heating time for different conditions of pressure and magnetic frequency: $P^* = 0.36$ and 25 atm; $f = 1$ and 5, with $k_{l,ef}^*$ and k_l^* for $T_\infty^* = 1000$ K .

Figure 5.10 shows the temperature profile in the thermal boundary layer at different heating times. The four upper curves represent the condition $p_m = 0.0134$ ($P^* = 0.36$ atm and $T_\infty^* = 1000$ K) for frequencies $f = 1$ and 5, considering the effective $k_{l,ef}^*$ and the pure liquid k_l^* thermal conductivity. The four curves below represent the condition $p_m = 0.928$ ($P^* = 25.0$ atm and $T_\infty^* = 1000$ K) for frequencies $f = 1$ and 5, considering the effective $k_{l,ef}^*$ and the pure liquid k_l^* thermal conductivity.

In order to compare the temperature profile for different conditions at a given heating time, the temperature was nondimensionalized by the boiling temperature of each case. The results put in evidence the effect of the effective thermal conductivity $k_{l,ef}^*$ in comparison to the pure liquid thermal conductivity k_l^* on the droplet heating for low and high pressure. For low pressure ($p_m = 0.0134$), the heating time is short because of two factors. The first one is that the initial droplet temperature $T_0^* = 297.24$ K is close to the boiling temperature $T_b^* = 338.9$ K which demands, comparatively to the high pressure cases, a small quantity of heat to heat up the droplet. The second factor is that large latent heat of vaporization in low pressure conditions imposes low vaporization rate practically during the whole heating process, resulting in low heat loss by vaporization. Since the effective thermal conductivity is larger than the

pure liquid thermal conductivity, the heat flux from the thermal boundary layer to the droplet core is large, which is reflected on larger temperatures on that region and lower temperature in the thermal boundary layer.

An increase of frequency increases the energy transferred from the external magnetic field to the magnetic nanoparticles, which leads to an increase on the temperature of the droplet core and the thermal boundary layer. The result is a short heating time, as seen in Fig. 5.10. However, the increase of temperature of the thermal boundary layer results in an increase of the heat flux from it to the droplet surface which elevates the vaporization rate and consequently the droplet heat loss. The energy balance shows a reduction on the temperature of thermal boundary layer which leads to longer heating time, as seen in Fig. 5.10.

By increasing the pressure from 0.36 atm to 25.0 atm ($p_m = 0.013$ to 0.93, practically two orders of magnitude) the heating time increases about two or four times, Fig 5.10. The reason for the increase of the heating time is the heating process to be followed simultaneously by vaporization. Since the droplet loses heat by vaporization, the boiling condition is reached later. For longer heating time, the heating process is exposed to the effect of thermal conductivity for a longer time. Using the effective thermal conductivity in the model, the droplet core has higher temperature at boiling condition, because more heat is transferred to the interior of the droplet. This fact is responsible for the boiling condition takes place later in comparison to the cases with the thermal conductivity of pure fuel k_l^* .

Figure 5.11 exhibits the relative temperature of the droplet surface as a function of time considering the pure and effective thermal conductivity for different pressures and frequencies. Figure 5.11 presents eight curves, in which the four in the upper side represent the condition $P^* = 0.36$ atm for $f = 1$ and 5 and the four curves below represent the condition $P^* = 25.0$ atm for $f = 1$ and 5, respectively. For low pressure, the latent heat is large enough to imposes vaporization only at temperatures close to the boiling temperature. For large thermal conductivity, more heat is transferred from the thermal boundary layer to the droplet core, then the temperature at the droplet surface is lower comparing to low thermal conductivity. This feature continues up to the maximum time, when the thermal boundary layer starts transferring heat to the droplet surface. Consequently, the vaporization rate and the temperature of the droplet surface increase. Unexpectedly, the final temperature of the droplet surface at heating time is the same for effective and pure liquid thermal conductivity.

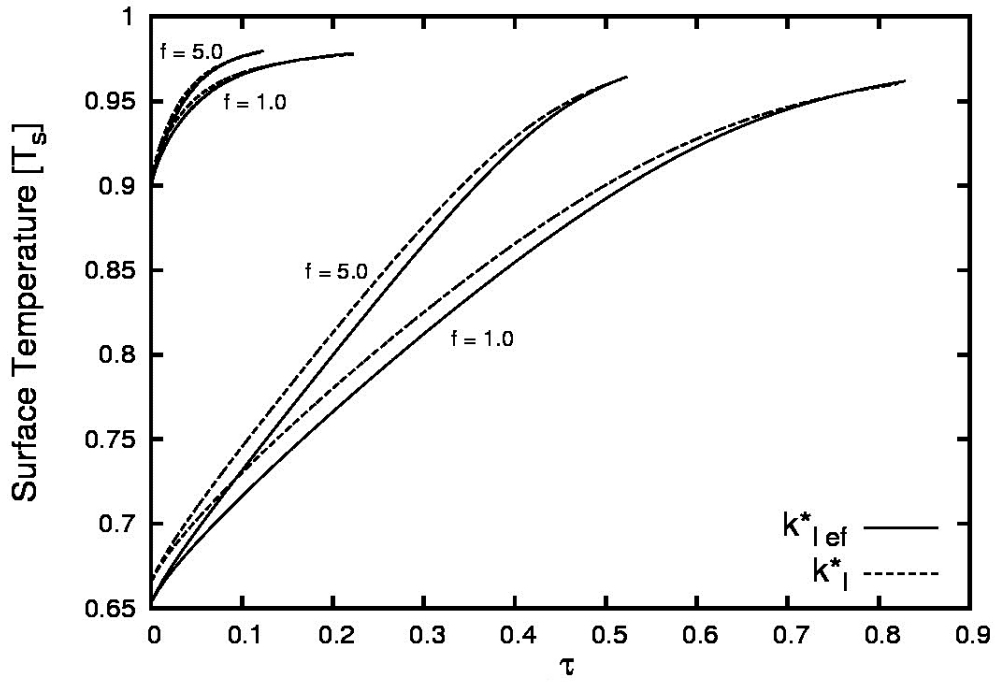


Figure 5.11 - Droplet surface temperature as a function of time for different conditions ($T_{\infty}^* = 1000$ K, $P^* = 0.36$ and 25 atm; $f = 1$ and 5), considering $k_{l,ef}^*$ and k_l^* .

Figure 5.12 shows the vaporization rate λ as a function of time. Upper curves represent $f = 5$ while the lower curves represent $f = 1$. As mentioned above, an increase on pressure and frequency lead to an augment on the vaporization rate because of a reduction on the latent heat and large amount of energy is transferred from the magnetic field to ferrofluid, respectively. The new feature observed in this figure is the vaporization for the cases considering effective thermal conductivity overpass that one for the cases considering pure liquid thermal conductivity. The reason for that is a larger heat flux provided in former cases from the thermal boundary layer to the droplet surface after the maximum time.

Analyzing the vaporization rate evolution as a function of pressure, a peculiar behavior is observed, Fig. 5.13.

Results point out an inversion on the vaporization rate evolution. Such behavior can be explained by analyzing the boiling temperature T_b and the latent heat of vaporization L^* as functions of pressure, Fig. 5.14.

For pressure regime below 10 atm the vaporization process is governed by the boiling temperature. Above that pressure, variations on the latent heat of vaporization

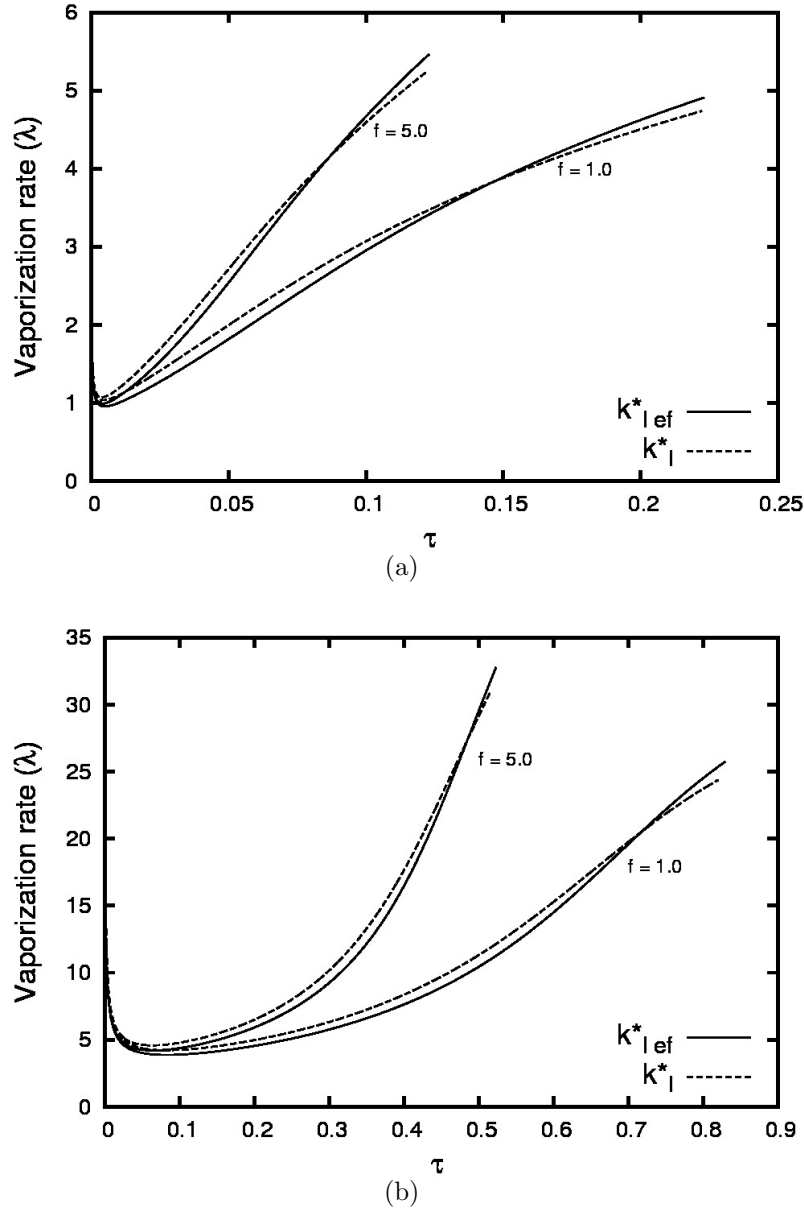


Figure 5.12 - Vaporization rate as a function of time a) low (0.36 atm) and b) high (25.0 atm) pressure ($T_\infty^* = 1000$ K and $f = 1$ and 5), considering $k_{l,ef}^*$ and k_l^* .

becomes more expressive making it the governing property. Furthermore, Figure 5.14 can be used to explain the great enhancement in the vaporization rates. As already mentioned, accumulative processes generate higher temperature gradients at the droplet surface, modifying the temperature profile inside the thermal boundary layer which enhances the vaporization rate. But at high pressure regimes higher boiling temperatures T_b and lower latent heats of vaporization L are found. Under that circumstances, the droplet achieve higher temperatures and lower heat quantity is necessary to transform the liquid into vapor. It justifies not only the inversion in

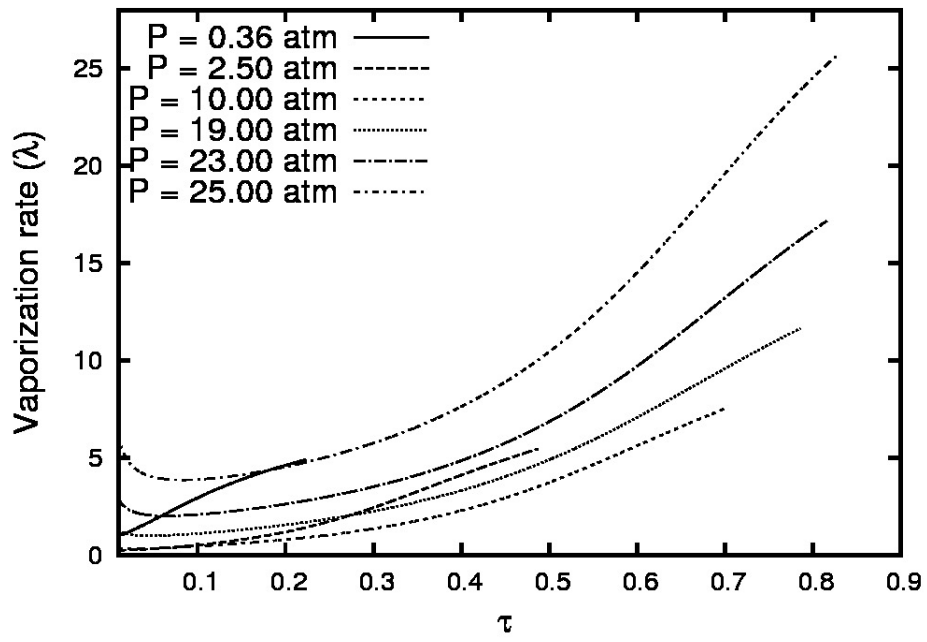


Figure 5.13 - Vaporization rate as a function of time for different pressure regime ($T_{\infty}^* = 1000$ K, $f = 1$)

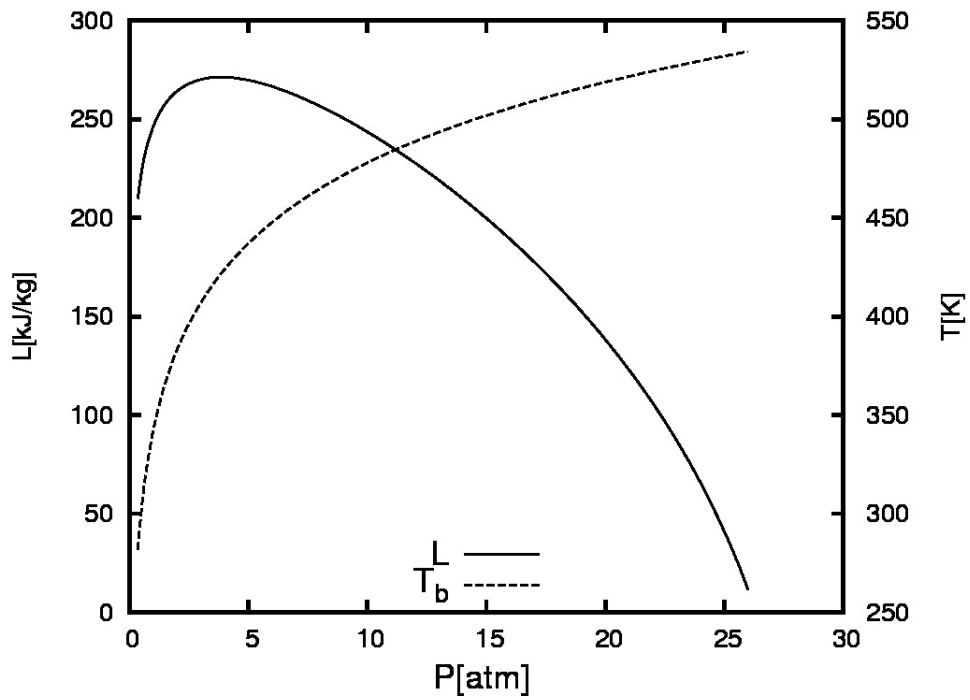


Figure 5.14 - Latent heat of vaporization and boiling temperature as a function of pressure ($T_{\infty}^* = 1000$ K, $f = 1$)

the vaporization rate but also the huge augment in the vaporization rate at high pressure regime.

Droplet explosion will be expected for situations in which the boiling condition is reached during the droplet lifetime. This droplet break up can be an extra mechanism to the atomization of liquid.

6 CONCLUSION AND FUTURE WORKS

The main objective of this work is to investigate the influence of the transient terms in the heating and vaporization of a ferrofluid droplet under a large alternated magnetic field. An analysis is performed under the condition of very large magnetic field ($P_m \gg 1$.) A thermal boundary layer is established adjacent to the droplet surface in the liquid side. The profiles of temperature inside the thermal boundary layer are obtained in appropriate time and length scales. The profiles of both phases (liquid and gas) are matched satisfying the boundary conditions at the droplet surface.

The heating and vaporization problem are solved by two models: 1) Constant property model, which considers the properties of the ferrofluid droplet all constants, assuming the properties of pure fuel for the droplet and 2) Variable property model, which considers the effective properties for the ferrofluid droplet with latent heat of vaporization and boiling temperature as functions of pressure.

The droplet heating and vaporization are dependent on the temperature profile inside the thermal boundary layer. Inside the thermal boundary layer a maximum of temperature is found at high ambient temperatures. This maximum on the temperature occurs due to the temperature dependence of the magnetic relaxation (which makes the temperature to increase faster in the thermal boundary layer than in the droplet core) and the heat loss at the droplet surface due to vaporization. At high ambient temperatures an extra heat flux is provided toward the droplet surface. As consequence, higher vaporization rates are shown. The transient processes in the gas phase are found to be significant on droplet heating and vaporization. Transient process, i.e., energy and mass accumulation in the gas phase around the droplet, improve the fluxes of heat and mass close to the droplet surface by maintaining the droplet exposed to high gradients for longer periods of time. That, can also be used to explain the increase in the vaporization rate. The ferrofluid droplet heating and vaporization are found to be dependent on the initial conditions of the problem.

The boiling condition is found inside the droplet, which can favor the formation of bubble and the disruption of the droplet. This situation is expected to be an extra atomization process.

6.1 Future works

This work is based on the asymptotic limit of $P_m \gg 1$, demanding magnetic fields with very large intensity. Such magnetic fields can only be produced by special

magnets. Also in this work only the ferrofluid droplet vaporization is studied. Taking those ideas in concern, some suggestions are presented:

- To consider the case of transient droplet combustion under the influence of a large magnetic field.
- To vary the Lewis number, which was considered equal unit in the current work ($Le_F = 1$).
- To consider cases of $P_m \sim O(1)$, in which the hypothesis of very low radius variation will not be valid.

REFERENCES

- BURKE, S. P.; SCHUMANN, T. E. W. Diffusion flames. **Industrial and Engineering Chemistry**, v. 20, p. 998 – 1004, 1928. [3](#)
- CHEN, H.; DING Y.L., H. Y.; TAN, C. Rheological behaviour of ethylene glycol based titania nanofluids. **Chemical Physical Letters**, v. 444, p. 333 – 337, 2007. [8](#)
- CHOI, S. U. S. Enhancing thermal conductivity of nanofluids with nanoparticles. **Developments and Applications of Non-Newtonian Flows**, 1995. [6](#)
- CHOI, S. U. S.; ZHANG, Z. G.; YU, W.; LOCKWOOD, F. E.; GRULKE, E. A. Anomalous thermal conductivity enhancement in nanotube suspensions. **Applied Physics Letter**, n. 79, 2001. [8](#)
- CRESPO, A.; LINÀN, A. Unsteady effects in droplet evaporation and combustion. **Combustion Science and Technology**, v. 11, p. 9 – 18, 1975. [5](#)
- CRISTALDO, C. C.; FACHINI, F. F. Asymptotic analysis of ferrofluid droplet combustion under very large magnetic power. **Combustion and Flame**, v. 160, n. 8, p. 1458–1465, 2013. [10](#), [11](#), [17](#), [19](#), [22](#), [30](#), [32](#), [35](#), [36](#), [40](#)
- CRISTALDO, C. F. C.; FACHINI, F. F. Ferrofluid droplet heating and vaporization under very large magnetic power: A thermal boundary layer model. **Physics of Fluids**, v. 25, n. 3, 2013. [10](#), [11](#), [17](#), [19](#), [22](#), [30](#), [32](#), [39](#), [40](#)
- DAS, S. K.; PUTRA, N.; THIESEN, P.; ROETZEL, W. Temperature dependence of thermal conductivity enhancement for nanofluids. **Journal of Heat Transfer**, v. 125, p. 567 – 574, 2003. [6](#)
- DING, Y.; CHEN, H.; WANG, L.; YANG, C.-Y.; HE, Y.; YANG, W.; LEE, W. P.; ZHANG, L.; HUO, R. Heat transfer intensification using nanofluids. **KONA Powder and Particle Journal**, v. 25, n. 25, p. 23–38, 2007. [7](#)
- EASTMAN, J. A.; CHOI, S. U. S.; LI, S.; YU, W.; THOMPSON, L. Anomalously increased effective thermal conductivities of ethylene glycol-based nanofluids containing copper nanoparticles. **Applied Physics Letter**, v. 78, n. 6, p. 718–720, 2001. [7](#), [8](#)
- EVANS, W.; FISH, J.; KEBLISNKI, P. Role of brownian motion hydrodynamics on nanofluids thermal conductivity. **Applied Physical Letters**, v. 88, 2006. 093116. [7](#)

- FACHINI, F. F. Effects of the initial droplet temperature on the vaporization process at high pressure. **Journal of the Brazilian Society of Mechanical Sciences and Engineering**, v. 29, n. 1, p. 91 – 98, 2007. [3](#), [5](#)
- FACHINI, F. F.; BAKUZIS, F. Decreasing nanofluid droplet heating time with alternating magnetic fields. **Journal of Applied Physics**, v. 108, n. 084309, 2010. [10](#), [11](#), [17](#), [18](#), [19](#), [30](#), [32](#)
- FACHINI, F. F.; LINÀN, A.; WILLIAMS, F. A. Theory of flame histories in droplet combustion at small stoichiometric fuel-air ratios. **American Institute of Aeronautics and Astronautics Journal**, v. 37, p. 1426 – 1435, 1999. [5](#)
- FAETH, G. M. Current status of droplet and liquid combustion. **Progress in Energy and Combustion Science**, v. 3, p. 191–224, 1977. [4](#)
- FERZIGER, J. H.; PERIC, M. **Computational Methods for Fluid Dynamics**. [S.l.]: Springer, 2002. [26](#), [27](#)
- FISHTINE, S. H. Reliable latent heats of vaporization. **Industrial and Engineering Chemistry**, v. 55, n. 6, 1963. [38](#)
- FRÖSSLING, N. On the evaporation of falling drops. **Gearlands Beiträge Zur Geophysik**, v. 52, p. 170 – 175, 1938. [3](#)
- GHADIMI, A. A review of nanofluids stability properties and characterization in stationary conditions. **International Journal of Heat and Mass Transfer**, v. 54, n. 17-18, p. 4051–4068, 2011. [7](#)
- GODSAVE, G. A. E. Studies on the combustion of drops in a fuel spray - the burning of single drops fuel. **Proceedings of the Combustion Institute**, v. 4, p. 818 – 830, 1953. [3](#)
- GOLDSMITH, M.; PENNER, S. S. On the burning of single drops of fuel in an oxidizing atmosphere. **Jet Propulsion**, v. 24, p. 245 – 251, 1954. [3](#), [4](#)
- HAGGENMACHER, J. E. An equation for the line of saturation of liquids and vapors. **Journal of the American Chemical Society**, v. 68, p. 1633, 1946. [37](#)
- ISODA, H.; KUMAGAI, S. New aspect of droplet combustion. **Proceedings of the Combustion Institute**, p. 523 – 531, 1958. [5](#)
- JIA, H.; GOGOS, G. Droplet vaporization in subcritical and supercritical environments; high vs low pressure modelling. **Acta Astronautica**, v. 32, n. 2, p. 121 – 129, 1994. [5](#)

JORDAN, A. Magnetic fluid hyperthermia (mfh): Cancer treatment with ac magnetic field induced excitation of biocompatible supermagnetic nanoparticles. **Journal of Magnetism and Magnetic Materials**, v. 85, p. 233, 1999. [9](#)

KAPPIYOOR, R. The effects of magnetic nanoparticle properties on magnetic fluid hyperthermia. **Journal of Applied Physics**, v. 108, 2010. 094702. [9](#)

KEBLINSKI, P. **Nanofluids for enhanced thermal transport: understanding and controversy**. San Francisco, USA: [s.n.], 2007. [7](#), [8](#)

KEBLINSKI, P.; CAHILL, D. **Comment on "model for heat conduction in nanofluids"**. 2005. 209401. [7](#)

KEBLINSKI, P.; PHILLPOT, S. R.; CHOI, S. U. S.; EASTMAN, J. A. Mechanisms of heat flow in suspensions of nano-sized particles (nanofluids). **International Journal of Heat and Mass Transfer**, v. 45, p. 855–863, 2002. [6](#), [7](#)

KEBLINSKI, P.; PRASHER, R.; EAPEN, J. Thermal conductance of nanofluids: is the controversy over? **Journal of Nanoparticle Research**, n. 10, 2008. [8](#)

KOBAYASHI, K. A study on the evaporation and combustion of a single droplet. **The Japan Society of Mechanical Engineers**, 1954. [4](#)

KOO, J.; KLEINSTREUER, C. A new thermal conductivity model for nanofluids. **Journal of Nanoparticle Research**, v. 6, p. 577 – 588, 2005. [7](#)

KOO, J.-Y.; MARTIN, J. K. **Droplet sizes and velocities in a transient diesel fuel spray**. Detroit, Michigan: [s.n.], 1990. Technical paper. [2](#)

KUMAR, D.; PATEL, H.; KUMAR, V.; SUNDARARAJAN, T.; PRADEEP, T.; DAS, S. Model for heat conduction in nanofluids. **Physical Review Letter**, v. 93, 2004. [7](#)

LEE, S.; CHOI, S. U. S.; LI, S.; EASTMAN, J. A. Mesuring thermal conductivity of fluids containing oxide nanoparticles. **Journal of Heat Transfer**, v. 121, p. 280–289, 1999. [8](#)

LEFEBVRE, A. H. Atomization. **A-to-Z Guide to Thermodynamics, Heat and Mass Transfer, and Fluids Engineering**, 2011. DOI:10.1615/AtoZ.a.atomization. [1](#), [2](#)

MAENOSONO, S.; SAITA, S. Theoretical assessment of fept nanoparticles as heating elements for magnetic hyperthermia. **IEEE Transactions on Magnetism**, v. 42, p. 1638 – 1642, 2006. [38](#)

MARCHESE, A. J.; DRYER, F. L. The effect of liquid mass transport on the combustion and extinction of bi-component droplets of methanol and water. **Combustion and Flame**, v. 105, p. 104 – 122, 1996. [4](#)

MASUDA, H.; EBATA, A.; TERAMAE, K.; HISHINUMA, N. Alteration of thermal conductivity and viscosity of liquid by dispersing ultra fine particles (dispersion of $\gamma - \text{Al}_2\text{O}_3$, SiO_2 , and TiO_2 ultra fine particles). **Netsu Bussei (Japan)**, v. 4, p. 227 – 233, 1993. [8](#)

MAXWELL, J. **A Treatise on electricity and magnetism, second ed.** Oxford, UK: Clarendon Press, 1881. [6](#)

MERZHANOV, A. G. Fundamentals, achievements, and perspectives for development of solid-flame combustion. **Russian Chemical Bulletin**, v. 46, n. 1, p. 8 – 32, 1997. [1](#)

OFFICE OF ADVANCED RESEARCH AND TECHNOLOGY, NATIONAL AERONAUTICS AND SPACE ADMINISTRATION. **Study of ferromagnetic liquid / by R.E. Rosensweig and R. Kaiser.** Washington, D.C., 1967. NTIS Report No. NASW-1219. [8](#), [9](#)

OZAKI, T.; GOMI, M. The combustion and evaporation of a fuel droplet. **The Japan Society of Mechanical Engineers**, 1953. [3](#)

PAPELL, S. S. U.s patent number 3. 1965. 572, 215. [8](#), [9](#)

PATEL, H. E.; DAS, S. K.; SUNDARARAJAN, T.; NAIR, A. S.; GEORGE, B.; PRADEEPA, T. Thermal conductivities of naked and monolayer protected metal nanoparticle based nano- fluids: Manifestation of anomalous enhancement and chemical effects. **Applied Physical Letters**, v. 83, p. 2931–2933, 2003. [7](#)

PEREZ-CASTILLEJOS, R.; PLAZA, J.; ESTEVE, J.; LOSANTOS, n. M. A. P.; CANE, C.; SERRA-MESTRES, F. The use of ferrofluids in micromechanics. **Sensors and Actuators**, v. 84, 2000. [9](#)

PFEFFERLE, W.; PFEFFERLE, L. Catalytically stabilized combustion. **Progress in Energy and Combustion Science**, v. 12, 1986. [1](#)

PHILIP, J.; SHIMA, P. D.; RAJ, B. Enhancement of thermal conductivity in magnetite based nanofluid due to chainlike structures. **Applied Physics Letter**, n. 91, 2007. 8

PRAKASH, S. V.; SHANKAPAL, S. R. Experimental investigation of combustion of biomass slurry in an oil fired furnace. In: INTERNATIONAL SOLAR ENERGY SOCIETY. **Proceedings of ISES World Congress**. [S.l.], 2007. p. 2400–2404. 6

PRASHER, R.; BHATTACHARYA, P.; PHELAN, P. E. Thermal conductivity of nanoscale colloidal solutions (nanofluids). **Physical Review Letters**, v. 94, 2005. 025901. 7

PRASHER, R.; EVANS, W.; MEAKIN, P.; FISH, J.; PHELAN, P.; KEBLINSKI, P. Effect of aggregation on thermal conduction in colloidal nanofluids. **Applied Physics Letters**, v. 89, 2006. 7, 8

RAJ, K. Commercial applications of ferrofluids. **Journal of Magnetism and Magnetic Materials**, v. 85, p. 233, 1990. 9

RAYLEIGH, L. On instability of jets. **Proceedings of the London Mathematical Society**, v. 10, p. 4–13, 1878. DOI:10.1112/plms/s1-10.1.4. 2

ROSENSWEIG, R. E. **Ferrohydrodynamics**. [S.l.]: Cambridge University Press, 1985. 8, 9, 18, 19

_____. Heating magnetic fluid with alternating magnetic field. **Journal of Magnetic Materials**, p. 370–374, 2002. 9

SAMI, H.; OGASAWARA, M. Study on the burning of a fuel drop in heated and pressurized air stream. **Bulletin of the Japan Society of Mechanical Engineers**, v. 13, n. 57, p. 395–404, 1970. 4

SCHERER, C.; NETO, A. M. F. Ferrofluids: Properties and applications. **Brazilian Journal of Physics**, v. 35, 2005. 10

SHENOGIN, S.; BODAPATI, L. X. A.; OZISIK, R.; KEBLINSKI, P. Effect of chemical functionalization on thermal transport of carbon nanotube composites. **Applied Physics Letters**, v. 85, p. 2229–2231, 2004. 7

SHENOGIN, S.; XUE, L.; OZISIK, R.; KEBLINSKI, P.; CAHILL, D. Role of thermal boundary resistance on the heat flow in carbon nanotube composites. **Journal of Applied Physics**, v. 95, p. 8136–8114, 2004. 7

SHIMA, P. D.; PHILIP, J.; RAJ, B. Role of microconvection induced by brownian motion of nanoparticles in the enhanced thermal conductivity of stable nanofluids. **Applied Physics Letter**, v. 94, 2009. [8](#)

SIRIGNANO, W. A. Fuel droplet vaporization and spray combustion. **Progress in Energy and Combustion Science**, v. 9, p. 291 – 322, 1983. [4](#)

_____. **Fluid Dynamics and Transport of Droplets and Sprays**. The Edinburgh Building, Cambridge CB2 2RU, UK: Cambridge University Press, 1999. [3](#), [4](#)

SPALDING, D. B. The combustion of liquid fuels. **Proceedings of the Combustion Institute**, v. 4, n. 1, p. 847 – 864, 1953. [3](#)

SZEKELY, J. G. A. **Experimental Evaluation of a Carbon Slurry Droplet Combustion Model**. Doctoral thesis — The Pennsylvania State University, Applied Research Laboratory, P.O. Box 30, State College, PA 16801, 1981. [6](#)

TAYLOR, R.; COULOMBE, S.; OTANICAR, T.; PHELAN, P.; GUNAWAN, A.; LV, W.; ROSENGARTEN, G.; PRASHER, R.; TYAGI, H. Critical review of the novel applications and uses of nanofluids. **Proceedings of the ASME 2012 3rd Micro/Nanoscale Heat and Mass Transfer International Conference**, Atlanta, Georgia, USA, 2012. [6](#), [7](#), [8](#)

TYAGI, H.; PHELAN, P. E.; PRASHER, R.; PECK, R.; LEE, T.; PACHECO, J. R.; ARENTZEN, P. Increased hot-plate ignition probability for nanoparticle-laden diesel fuel. **Nano Letters**, v. 8, n. 5, p. 1410 – 1416, 2008. [8](#)

WALDMAN, C. H. Theory of non-steady state droplet combustion. **Proceedings of the Combustion Institute**, v. 15, p. 429–442, 1975. [5](#)

WANG, B. X.; ZHOU, L. P.; PENG, X. F. A fractal model for predicting the effective thermal conductivity of liquid with suspension of nanoparticles. **International Journal of Heat and Mass Transfer**, v. 46, p. 2665–2672, 2003. [7](#)

WANG, X.-Q.; MUJUMDAR, A. S. Heat transfer characteristics of nanofluids: a review. **International Journal of Thermal Sciences**, 2007. [7](#)

WEBER, C. Disintegration of liquid jets. **Journal of Applied Mathematics and Mechanics**, v. 11, n. 2, p. 136–159, 1931. DOI:10.1002/zamm.19310110207. [2](#)

WILLIAMS, A. Combustion of droplets of liquid fuels: A review. **Combustion and Flame**, v. 21, p. 1 – 31, 1973. [4](#)

WISE, H. The effects of chemical and physical parameters on the burning rate of a liquid droplet. **Proceedings of the combustion Institute**, v. 24, p. 132 – 141, 1955. [3](#)

WONG, K. V.; LEON, O. D. Applications of nanofluids: Current and future. **Advances in Mechanical Engineering**, 2010. [8](#)

YETTER, R. A.; RISHS, G. A.; SON, S. F. **Proceedings of the Combustion Institute**, n. 32, 2009. [8](#)

YU, C.; RICHTER, A.; DATTA, A.; DURBIN, M.; DUTTA, P. Molecular layering in a liquid on a solid substrate: an x-ray reflectivity study. **Physica B**, v. 293, p. 27–31, 2000. [38](#)

YU, W.; CHOI, S. U. S. The role of interfacial layers in the enhanced thermal of nanofluids: a renovated maxwell model. **Journal of Nanoparticle Research**, v. 5, n. 1-2, p. 167–171, 2003. [7](#), [38](#)

APPENDIX

A.1 Vaporization rate

Considering a spherical droplet then the mass variation inside it is equal to the vaporization rate

$$\dot{m}_F^* = -\frac{dm^*}{dt^*} \quad (\text{A.1})$$

in which F means fuel.

It is possible to re-write the above equation, knowing that

$$m = \rho_l^* V^* \quad (\text{A.2})$$

in which V is the sphere volume $V = 4\pi r^3/3$. Then

$$\dot{m}_F^* = -\frac{4\pi\rho_l^*}{3} \frac{dr^3}{dt^*} \quad (\text{A.3})$$

The droplet radius is a time dependent variable and will be denoted by $a^*(t^*)$, then

$$\dot{m}_F^* = -\frac{4\pi\rho_l^*}{3} \frac{d[a^*(t^*)^3]}{dt^*}$$

Re-writing the previous equation

$$\frac{da^{*3}}{dt^*} = -\frac{3}{4} \frac{\dot{m}_F^*}{\pi\rho_l^*} \quad (\text{A.4})$$

A.2 Adimensionalization

The equations are made non-dimensional by use of the following dimensionless variables

$$t \equiv t^*/t_h^*, \quad \rho \equiv \rho^*/\rho_\infty^*, \quad r \equiv r^*/a_0^*, \quad T \equiv T^*/T_b^*, \quad u \equiv u^*/(\alpha_\infty^*/a_0^*), \quad a \equiv a^*/a_0^*$$

in which the heating time estimative is $t_h^* \equiv \rho_l^* a_0^{*2} / (\rho_\infty^* \alpha_\infty^*)$ and the thermal diffusivity is $\alpha_\infty^* \equiv k_\infty^* / (c_p^* \rho_\infty^*)$. The variable a^* the instantaneous dimensional droplet radius, a_0^* is the initial droplet radius, T_b^* is the droplet boiling temperature, ρ_∞^* is the gas phase density, c_p^* is the specific heat at a constant pressure and k_∞^* is the thermal conductivity of the gas phase.

$$\frac{\partial t}{\partial t^*} = \frac{\partial}{\partial t^*} \left(\frac{t^*}{t_h^*} \right) = \frac{1}{t_h^*} \frac{\partial t^*}{\partial t^*} = \frac{1}{t_h^*} \quad (\text{A.5})$$

$$\frac{\partial r}{\partial r^*} = \frac{\partial}{\partial r^*} \left(\frac{r^*}{a_0^*} \right) = \frac{1}{a_0^*} \frac{\partial r^*}{\partial r^*} = \frac{1}{a_0^*} \quad (\text{A.6})$$

Equations (A.5) and (A.6) are presented here to not become repetitive ahead.

A.2.1 Liquid phase

A.2.1.1 Mass conservation

Starting with Eq. (A.4)

$$\frac{da^{*3}}{dt^*} = -\frac{3 \dot{m}_F^*}{4 \pi \rho_l^*} \quad (\text{A.7})$$

$$\frac{dt}{dt^*} \frac{da^3}{dt} = -\frac{3}{4} \frac{\dot{m}_F^*}{\pi a_0^{*3} \rho_\infty^*} \quad (\text{A.8})$$

substituting Eq. (A.5) into Eq. (A.8)

$$\frac{da^3}{dt} = -3 \frac{c_p^* \dot{m}_F^*}{4 \pi a_0^* k_\infty^*} \quad (\text{A.9})$$

assuming $\lambda \equiv (c_p^* \dot{m}_F^*) / (4 \pi a_0^* k_\infty^*)$

$$\frac{da^3}{dt} = -3\lambda(t) \quad (\text{A.10})$$

A.2.1.2 Energy conservation

$$\frac{\partial}{\partial t}(\rho_l^* c_l^* T^*) = \frac{\partial}{\partial r^*} \left[r^{*2} k_l^* \frac{\partial T}{\partial r^*} \right] + \pi \mu_0^* \xi_0^* (H^*)_0^2 f^* \frac{2\pi f^* t_r^*}{1 + (2\pi f^* t_r^*)^2} \quad (\text{A.11})$$

Calling the whole source equals a F, then

$$\frac{\partial t}{\partial t^*} \frac{\partial}{\partial t}(\rho_l^* c_l^* T^*) = \frac{1}{r^2} \frac{\partial r}{\partial r^*} \frac{\partial}{\partial r} \left[r^2 k_l^* \frac{\partial r}{\partial r^*} \frac{\partial T^*}{\partial r} \right] + F \quad (\text{A.12})$$

substituting Eq.(A.5) and (A.6) into Eq.(A.12) and assuming ρ_l^* , k_l^* , and c_l^* constants, then

$$\frac{\rho_l^* c_l^* T_b^*}{t_h^*} \frac{\partial T}{\partial t} = \frac{k_l^* T_b^*}{a_0^{*2} r^2} \frac{\partial}{\partial r} \left[r^2 \frac{\partial T}{\partial r} \right] + F$$

$$\frac{\partial T}{\partial t} = \frac{k_l^*}{k_{g\infty}^*} \frac{c_p^*}{c_l^*} \frac{\partial}{\partial r} \left[r^2 \frac{\partial T}{\partial r} \right] + G$$

Assuming $A \equiv k_l^* c_p^* / (k_{g\infty}^* c_l^*)$, $G \equiv P_m f^2 \tau_r(T) / \{1 + [f \tau_r(T)]^2\}$ where $f \equiv 2\pi f^* t_{B_b}^*$ and $P_m \equiv \mu_0 \chi_0 H_0 t_h^* / (2\rho_l^* c_l^* T_b^* t_{B_b}^*)$. The term $\tau_r \equiv t_h^* / t_{B_b}^*$ is the non-dimensional Brownian relaxation time in which $t_{B_b}^*$ is the effective Brownian relaxation time determined at boiling temperature, μ_0 is the magnetic permeability, χ_0 is the magnetic susceptibility and H_0 the magnetic field amplitude. Re-writing the equation

$$\frac{\partial T}{\partial t} = \frac{A}{r^2} \frac{\partial}{\partial r} \left[r^2 \frac{\partial T}{\partial r} \right] + P_m \frac{f^2 \tau_r(T)}{1 + (f \tau_r(T))^2} \quad (\text{A.13})$$

or

$$\frac{1}{P_m} \frac{\partial T}{\partial t} = \frac{A}{P_m r^2} \frac{\partial}{\partial r} \left[r^2 \frac{\partial T}{\partial r} \right] + \frac{f^2 \tau_r(T)}{1 + (f \tau_r(T))^2}$$

Now re-scaling the equation by use of

$$\tau = P_m t \quad r = a + \delta x \quad \text{in which} \quad \delta \ll a(t)$$

therefore

$$\frac{\partial}{\partial t} = \frac{\partial}{\partial t} + \frac{\partial x}{\partial t} \frac{\partial}{\partial x} \quad \text{and} \quad \frac{\partial}{\partial r} = \frac{\partial x}{\partial r} \frac{\partial}{\partial x}$$

$$\frac{\partial}{\partial t} = \frac{\partial \tau}{\partial t} \frac{\partial}{\partial \tau}$$

with

$$\frac{\partial \tau}{\partial t} = \frac{\partial(P_m t)}{\partial t} = P_m$$

and

$$x = \frac{r - a}{\delta} \quad \text{and} \quad \frac{da}{d\tau} = \dot{a}$$

then

$$\frac{1}{P_m} \left[\frac{\partial}{\partial t} + \frac{\partial x}{\partial t} \frac{\partial}{\partial x} \right] (T) = \frac{A}{P_m(a + \delta x)^2} \frac{\partial x}{\partial r} \frac{\partial}{\partial x} \left[(a + \delta x)^2 \frac{\partial x}{\partial r} \frac{\partial T}{\partial x} \right] + \frac{f^2 \tau_r(T)}{1 + (f \tau_r(T))^2}$$

$$\frac{\partial x}{\partial r} = \frac{\partial}{\partial r} \left(\frac{r - a}{\delta} \right) = \frac{1}{\delta}$$

knowing that $a = a(\tau)$

$$\frac{\partial x}{\partial t} = \frac{\partial}{\partial t} \left(\frac{r - a}{\delta} \right) = -\frac{\partial}{\partial t} \left(\frac{a}{\delta} \right) = -\frac{1}{\delta} \frac{\partial a}{\partial t} = -\frac{1}{\delta} \frac{\partial a}{\partial t} \frac{\partial a}{\partial a} = -\frac{1}{\delta} \frac{\partial \tau}{\partial t} \frac{\partial a}{\partial \tau} \frac{\partial a}{\partial a} = -P_m \frac{\dot{a}}{\delta}$$

$$\frac{1}{P_m} \left[P_m \frac{\partial}{\partial \tau} - P_m \frac{\dot{a}}{\delta} \frac{\partial}{\partial x} \right] (T) = \frac{A}{P_m(a + \delta x)^2} \frac{1}{\delta} \frac{\partial}{\partial x} \left[(a + \delta x)^2 \frac{1}{\delta} \frac{\partial T}{\partial x} \right] + \frac{f^2 \tau_r(T)}{1 + (f \tau_r(T))^2}$$

expanding $(a + \delta x)^2$

$$(a + \delta x)^2 = \underbrace{a^2}_{O(1)} + \underbrace{2a\delta x}_{O(\ll 1)} + \underbrace{(\delta x)^2}_{O(\ll 1)}$$

and neglecting terms much smaller than one, the previous equation becomes:

$$\begin{aligned} \frac{1}{P_m} \left[P_m \frac{\partial}{\partial \tau} - P_m \frac{\dot{a}}{\delta} \frac{\partial}{\partial x} \right] (T) &= \frac{A}{P_m a^2} \frac{1}{\delta^2} \frac{\partial}{\partial x} \left[a^2 \frac{\partial T}{\partial x} \right] + \frac{f^2 \tau_r(T)}{1 + (f \tau_r(T))^2} \\ \frac{1}{P_m} \left[P_m \frac{\partial}{\partial \tau} - P_m \frac{\dot{a}}{\delta} \frac{\partial}{\partial x} \right] (T) &= \frac{A}{P_m \delta^2} \frac{\partial^2 T}{\partial x^2} + \frac{f^2 \tau_r(T)}{1 + (f \tau_r(T))^2} \\ \frac{\partial T}{\partial \tau} - \frac{\dot{a}}{\delta} \frac{\partial T}{\partial x} &= \frac{A}{P_m \delta^2} \frac{\partial^2 T}{\partial x^2} + \frac{f^2 \tau_r(T)}{1 + (f \tau_r(T))^2} \end{aligned} \quad (\text{A.14})$$

The first term in the right hand side of Eq. (A.14) need to be $O(1)$, otherwise there is no heat transfer inside the droplet. So in order guarantee the heat transfer $A/(P_m \delta^2) = O(1)$

$$\frac{A}{P_m} \frac{1}{\delta^2} = 1 \rightarrow \delta \equiv \left(\frac{A}{P_m} \right)^{\frac{1}{2}} \quad (\text{A.15})$$

substituting Eq.(A.15) into Eq.(A.14)

$$\begin{aligned} \frac{\partial T}{\partial \tau} - \frac{\dot{a}}{\left(\frac{A}{P_m} \right)^{\frac{1}{2}}} \frac{\partial}{\partial x} (T) &= \frac{A}{P_m \left[\left(\frac{A}{P_m} \right)^{\frac{1}{2}} \right]^2} \frac{\partial^2 T}{\partial x^2} + \frac{f^2 \tau_r(T)}{1 + (f \tau_r(T))^2} \\ \frac{\partial}{\partial \tau} (T) - \frac{\lambda}{2a^2 (AP_m)^{\frac{1}{2}}} \frac{\partial}{\partial x} (T) &= \frac{\partial^2 T}{\partial x^2} + \frac{f^2 \tau_r(T)}{1 + (f \tau_r(T))^2} \end{aligned}$$

while a small radius variation $a(\tau) \sim 1$, there is no risk of the multiplication $a^2 P_m$ be of $O(1)$ and the equation is valid. The second term in the left hand side of the previous equation is smaller than one, consequently this term will be neglected, resuming the equation to

$$\frac{\partial T}{\partial \tau} = \frac{\partial^2 T}{\partial x^2} + \frac{f^2 \tau_r(T)}{1 + (f \tau_r(T))^2}$$

For further simplification, is assumed that the energy dissipation is due to Brownian mechanism $\tau_r(T) \equiv 1/T$, resulting in

$$\frac{\partial T}{\partial \tau} = \frac{\partial^2 T}{\partial x^2} + \frac{f^2 T}{T^2 + f^2} \quad (\text{A.16})$$

A.2.2 Gas phase

A.2.2.1 Mass conservation

$$\frac{\partial}{\partial t^*}(\rho^* r^{*2}) + \frac{\partial}{\partial r^*}(r^{*2} \rho^* u^*) = 0 \quad (\text{A.17})$$

$$\rho_\infty^* a_0^{*2} \frac{\partial t}{\partial t^*} \frac{\partial}{\partial t}(\rho r^2) + a_0^{*2} \rho_\infty^* \alpha_\infty^* \frac{\partial r}{\partial r^*} \frac{\partial}{\partial r}(r^2 \rho u) = 0 \quad (\text{A.18})$$

substituting Eq.(A.5) and (A.6) into (A.18)

$$\frac{\rho_\infty^* a_0^{*2}}{t_h^*} \frac{\partial}{\partial t}(\rho r^2) + \rho_\infty^* \alpha_\infty^* \frac{\partial}{\partial r}(r^2 \rho u) = 0$$

recalling that $\alpha_\infty^* \equiv k_\infty^*/(c_p \rho_\infty^*)$ and $t_h^* \equiv \rho_l^* a_0^{*2}/(\rho_\infty^* \alpha_\infty^*)$, then

$$\varepsilon \frac{\partial}{\partial t}(\rho r^2) + \frac{\partial}{\partial r}(r^2 \rho u) = 0 \quad (\text{A.19})$$

in which $\varepsilon \equiv \rho_\infty^*/\rho_l^*$.

A.2.2.2 Energy conservation

$$\frac{\partial}{\partial t}(r^{*2} \rho^* T^*) + \frac{\partial}{\partial r^*}(r^{*2} \rho^* u^* T^*) = \frac{\partial}{\partial r^*} \left[r^{*2} k^* \frac{\partial T^*}{\partial r^*} \right] \quad (\text{A.20})$$

$$a_0^{*2} \rho_\infty^* T_b^* \frac{\partial t}{\partial t^*} \frac{\partial}{\partial t} (r^2 \rho T) + a_0^* \rho_\infty^* \alpha_\infty^* T_b^* \frac{\partial r}{\partial r^*} \frac{\partial}{\partial r} (r^2 \rho u T) = \quad (\text{A.21})$$

$$\frac{a_0^{*2} T_b^*}{c_p^*} \frac{\partial r}{\partial r^*} \frac{\partial}{\partial r} \left[r^2 k^* \frac{\partial r}{\partial r^*} \frac{\partial T}{\partial r} \right]$$

substituting Eqs.(A.5) and (A.6) into Eq.(A.21)

$$\frac{a_0^{*2}}{t_h^* \alpha_\infty^*} \frac{\partial}{\partial t} (r^2 \rho T) + \frac{\partial}{\partial r} (r^2 \rho u T) = \frac{\partial}{\partial r} \left[r^2 \frac{k^*}{k_\infty^*} \frac{\partial T}{\partial r} \right]$$

assuming $T^n \equiv k^*/k_\infty^*$, then

$$\varepsilon \frac{\partial}{\partial t} (r^2 \rho T) + \frac{\partial}{\partial r} (r^2 \rho u T) = \frac{\partial}{\partial r} \left[r^2 T^n \frac{\partial T}{\partial r} \right] \quad (\text{A.22})$$

A.2.2.3 Species conservation

$$\frac{\partial}{\partial t} (r^{*2} \rho^* Y_F) + \frac{\partial}{\partial r^*} (r^{*2} \rho^* u^* Y_F) = \frac{\partial}{\partial r^*} \left[r^{*2} \rho^* D_F^* \frac{\partial Y_F}{\partial r^*} \right] \quad (\text{A.23})$$

in which D_F is the mass diffusivity.

$$a_0^{*2} \rho_\infty^* \frac{\partial t}{\partial t^*} \frac{\partial}{\partial t} (r^2 \rho Y_F) + a_0^* \rho_\infty^* \alpha_\infty^* \frac{\partial r}{\partial r^*} \frac{\partial}{\partial r} (r^2 \rho u Y_F) = \quad (\text{A.24})$$

$$a_0^{*2} \rho_\infty^* \frac{\partial r^*}{\partial r} \frac{\partial}{\partial r^*} \left[r^2 \rho D_F \frac{\partial r}{\partial r^*} \frac{\partial Y_F}{\partial r} \right]$$

Substituting Eqs.(A.5) and (A.6) into Eq.(A.24)

$$\frac{a_0^{*2} \rho_\infty^*}{t_h^*} \frac{\partial}{\partial t} (r^2 \rho Y_F) + \rho_\infty^* \alpha_\infty^* \frac{\partial}{\partial r} (r^2 \rho u Y_F) = \rho_\infty^* \frac{\partial}{\partial r} \left[r^2 \rho D_F^* \frac{\partial Y_F}{\partial r} \right]$$

Re-arranging the previous equation knowing that $D_{F\infty}^*/\alpha_\infty^* = 1/Le_F$, then

$$\varepsilon \frac{\partial}{\partial t}(r^2 \rho Y_F) + \frac{\partial}{\partial r}(r^2 \rho u Y_F) = \frac{\partial}{\partial r} \left[\frac{r^2 D_F^* \rho}{L e_F D_{F\infty}^*} \frac{\partial Y_F}{\partial r} \right]$$

$$\varepsilon \frac{\partial}{\partial t}(r^2 \rho Y_F) + \frac{\partial}{\partial r}(r^2 \rho u Y_F) = \frac{\partial}{\partial r} \left[\frac{r^2 T^n}{L e_F} \frac{\partial Y_F}{\partial r} \right] \quad (\text{A.25})$$

in which $T^n \equiv \rho^* D_F^* / \rho_\infty^* D_{F\infty}^*$.

PUBLICAÇÕES TÉCNICO-CIENTÍFICAS EDITADAS PELO INPE

Teses e Dissertações (TDI)

Teses e Dissertações apresentadas nos Cursos de Pós-Graduação do INPE.

Manuais Técnicos (MAN)

São publicações de caráter técnico que incluem normas, procedimentos, instruções e orientações.

Notas Técnico-Científicas (NTC)

Incluem resultados preliminares de pesquisa, descrição de equipamentos, descrição e ou documentação de programas de computador, descrição de sistemas e experimentos, apresentação de testes, dados, atlas, e documentação de projetos de engenharia.

Relatórios de Pesquisa (RPQ)

Reportam resultados ou progressos de pesquisas tanto de natureza técnica quanto científica, cujo nível seja compatível com o de uma publicação em periódico nacional ou internacional.

Propostas e Relatórios de Projetos (PRP)

São propostas de projetos técnico-científicos e relatórios de acompanhamento de projetos, atividades e convênios.

Publicações Didáticas (PUD)

Incluem apostilas, notas de aula e manuais didáticos.

Publicações Seriadas

São os seriados técnico-científicos: boletins, periódicos, anuários e anais de eventos (simpósios e congressos). Constam destas publicações o Internacional Standard Serial Number (ISSN), que é um código único e definitivo para identificação de títulos de seriados.

Programas de Computador (PDC)

São a seqüência de instruções ou códigos, expressos em uma linguagem de programação compilada ou interpretada, a ser executada por um computador para alcançar um determinado objetivo. Aceitam-se tanto programas fonte quanto os executáveis.

Pré-publicações (PRE)

Todos os artigos publicados em periódicos, anais e como capítulos de livros.